MOLECULAR DESIGN OF NANOSTRUCTURED CATALYSTS FOR INDUSTRIAL REACTIONS

INTRODUCTION

Zeolites are widely used on a large scale and in a wide range of applications. The majority of them are used as ion exchangers in laundry detergents to remove calcium and magnesium ions from the water by exchanging these ions with sodium ions which are present in the zeolites. Furthermore, zeolites are applied as adsorbents in the purification of gas streams to remove water and volatile organic species, and in the separation of different isomers and gas-mixtures. They are applied also in the cleaning of radioactive waste. In this thesis project, the focus will be on one of the most important and valuable applications called "the catalysis" of zeolites.

Zeolites have an aluminosilicate framework with their structures consisting of silicon cations (Si^{4+}) and aluminum cations (Al^{3+}) surrounded by four oxygen anions (O^{2-}). Each oxygen anion connects two cations and this yields a three-dimensional framework, with a net negative charge of AlO_2^- tetrahedral building blocks. This charge comes from the difference in the valences between the silicon- and aluminum cations. It will be located on one of the oxygen anions connected to an aluminum cation, and then compensated by additional cations such as sodium ion (Na^+). For catalytic applications, almost all of the sodium ions are replaced by protons (H^+), which form a bond with the negative charge of oxygen anions. They are then called the "bridging oxygen" of the zeolite. This occurs on the Brønsted acid sites, as displayed in Figure 1, and are highly active in the catalytic cracking (Al-Baghli *et al.*, 2005, Gomez *et al.*, 2005, Triantafyllidis *et al.*, 2006), alkylation (Becker *et al.*, 1973, Corma *et al.*, 2000, Degnan Jr *et al.*, 2001, Du *et al.*, 2002, Reddy *et al.*, 1993, Siffert *et al.*, 2000), oligomerizaiton (Geobaldo *et al.*, 1997, Hsia Chen *et al.*, 1996, Svelle *et al.*, 2004), and isomerization reactions (Klepel *et al.*, 2003, Martins *et al.*, 2005).

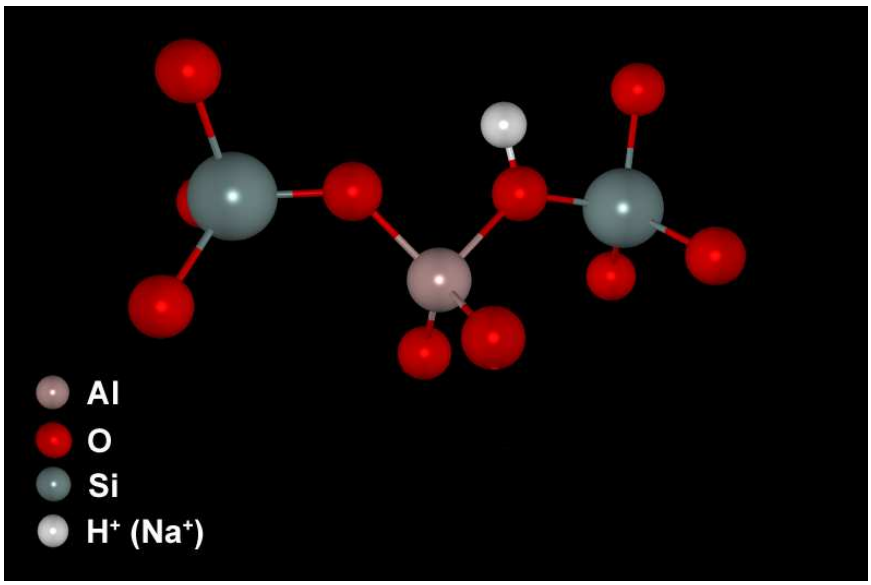

Figure 1 The Brønsted acid site of catalytic zeolite.

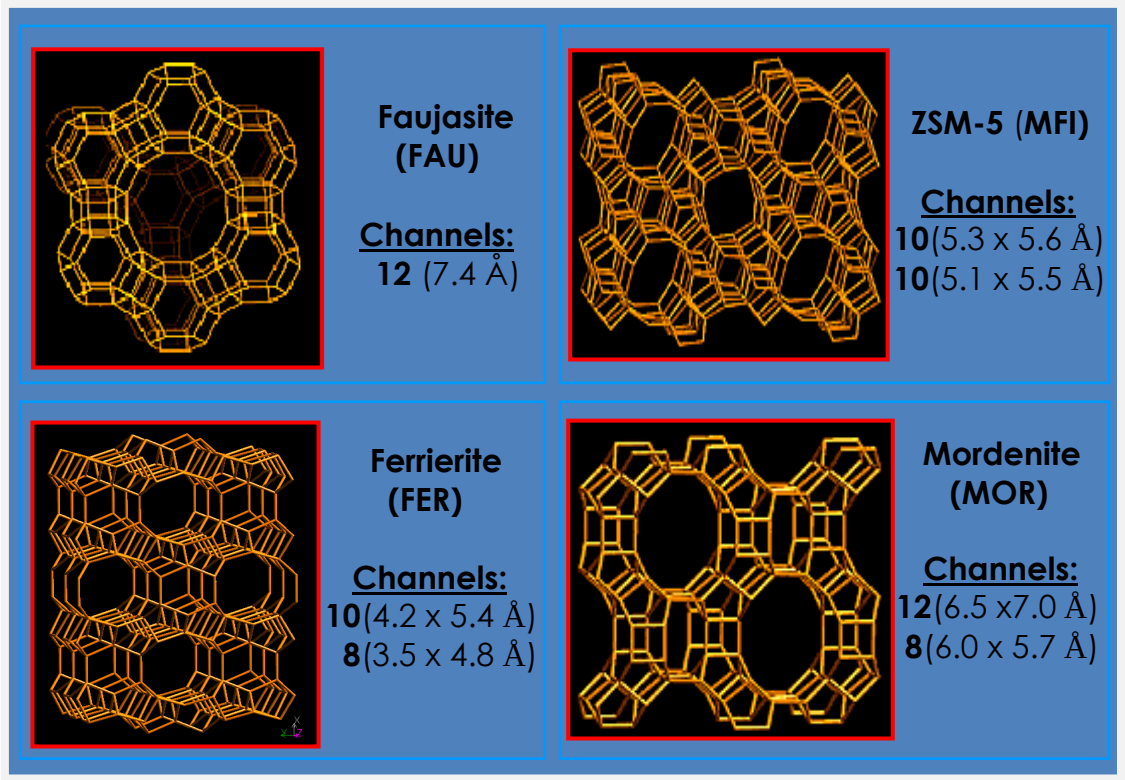

Figure 2 Various types of zeolite pores and channels (Figure credit; http://www.iza-sc.ethz.ch/IZA-SC/AtlasHome.html).

The structure of zeolite is a pore system with channels in one-, two- or three-dimensions. The diameters of the pores and cavities are in nanoscale with the range of 3-12 Å. The exact diameter of the pore depends on the coordination and the amount of cations and anions in the ring channel. The structures of four different zeolites are depicted in Figure 2. Faujasite (FAU) is a three-dimensional zeolite with large cavities present in the structure that are interconnected by 12-membered ring channels, which means that there are 12 cations (Si^{4+} and Al^{3+}) and 12 O^{2-} anions present in the ring. Ferrierite (FER) is a two-dimensional zeolite with 10-membered ring main channels, which are interconnected via smaller 8-membered ring side channels. For ZSM-5 (MFI) zeolite, the straight 10-membered ring channels are interconnected by 10-membered ring zigzag channels, which make this zeolite three-dimensional. Mordenite (MOR) is a 12-membered ring zeolite with the channels running in only one dimension. The 12-membered ring channels contain small 8-membered ring side-pockets. These pores and channels match with the dimensions of many hydrocarbon molecules. In this thesis project, the focus will be on the zeolites faujasite and ZSM-5, which are used as the catalysts in the important industrial reactions listed below.

1. Alkylation of benzene and ethylene to ethylbenzene

Ethylbenzene is an important raw material in the petrochemical industry for the manufacture of styrene, which is one of the most important industrial monomers. Worldwide capacity of ethylbenzene production is about 23 million metric tons per year (Degnan Jr *et al.,* 2001). Conventionally, ethylbenzene is produced by benzene alkylation with ethylene using mineral acids such as aluminum chloride or phosphoric acid as catalysts. However, these corrosive catalysts cause a number of problems concerning handling, safety, corrosion, and waste disposal. An immense endeavor has been put into developing alternative catalytic systems that are more environmentally friendly. As a result, the ethylbenzene production technology has been progressively moved toward zeolite based processes.

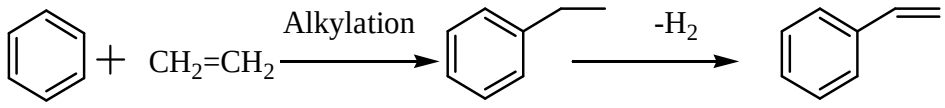

Figure 3 The alkylation of benzene with ethylene to ethylbenzene and the dehydrogenation of ethylbenzene to styrene.

Several types of zeolites have been reported to have high activity for benzene alkylation, for example, faujasite, beta, H-ZSM-5, and MCM-22 (Corma *et al.,* 2000, Morita *et al.,* 1973, Venuto *et al.,* 1966, Weitkamp 1985). Elucidation of the reaction mechanism of benzene alkylation on zeolite catalysts is of great interest. From an industrial point of view, understanding the alkylation mechanism could help in optimizing the reaction conditions and in designing a new catalyst for a more efficient process. To clearly envision the reaction mechanism, theoretical study can offer a practical tool that provides insight to the reaction mechanism complementing experimental investigations or, in certain cases, offer an understanding that is not possible by experimental investigation. Therefore, in this part of the thesis project, the theoretical study of the reaction mechanism of the alkylation of benzene with ethylene on an acidic faujasite zeolite has been employed.

2. Dimerization of ethylene

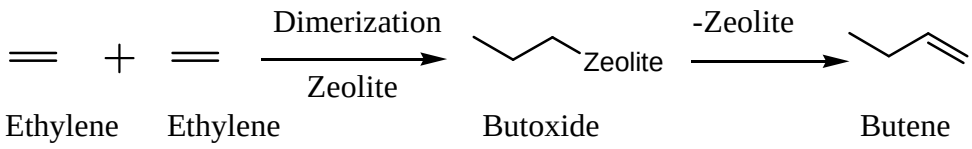

Figure 4 The dimerization of ethylene to butene.

Acid-catalyzed alkene dimerization and oligomerization are important reactions in industrial chemical processes because they result in C–C bond formation leading to higher hydrocarbons and, thus, can be used for the production of fuels and lubricants from light alkenes (Knifton *et al.,* 1994, O'Connor *et al.,* 1990). Linear

alkenes are produced by oligomerization of light alkenes in zeolite pores (Jeong *et al.*, 1998, Van Den Berg *et al.*, 1983) due to the constraints of the zeolite pore systems. Therefore, understanding the interactions of alkenes with acidic zeolites and dimerization as well as oligomerization in zeolite pore systems is of fundamental importance, because they are key steps in many important reactions catalyzed by zeolites (Bibby *et al.*, 1992, Corma 1995, Kiricsi *et al.*, 1999, Klepel *et al.*, 2003), for example, alkene oligomerization, alkylation of benzene with alkenes, and methanol-to-gasoline conversion. This part of the thesis project presents a theoretical study on the mechanism of ethylene dimerization in faujasite zeolite.

3. Isomerization of propene oxide

Epoxides are important intermediates for organic synthesis and for the chemical and petrochemical industries. With their high ring constraint, epoxides are very reactive, giving them extensive use for the syntheses of complex organic compounds, polymers, and macromolecules (Carlier 2004, Cheng *et al.*, 2005, Katsuki *et al.*, 1980, Smith 1984) via the ring-opening and isomerization reactions. The isomerization of unsymmetrical epoxides can give two different carbonyl compounds. For example, isomerization of propene oxide produces propanal and propanone (Figure 5). The major product is propanal, which results from the breaking of the more sterically hindered C-O bond of the epoxide ring.

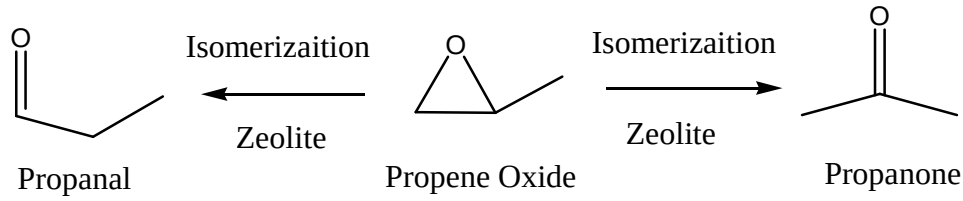

Figure 5 The isomerization of propene oxide to propanal and propanone.

For chemical processes, these reactions were conventionally catalyzed by Lewis acid catalysts ($AlCl_3$, and BF_3, etc.) that are highly toxic and corrosive and, consequently, present a serious waste disposal problem. To substitute the

conventional catalysts to reduce these problems, solid catalysts, for example, Al_2O_3, Al_2O_3-SiO_2, ZnO (Molnar *et al.*, 1991) Nafion-H (Fasi *et al.*, 2004), zeolites (Fasi *et al.*, 2001), and so forth, have been developed. Among these solid catalysts, zeolites are considered to be one of the most promising alternatives because they can be reused and reactivated. Acidic zeolites are active in the isomerization of propene oxide. The reactions occur on Brønsted or Lewis acid sites. The confined environment of zeolites also favors the dimerization. The product distribution strongly depends on the pore sizes of the zeolites (Fasi *et al.*, 2001).

In the Results and Discussion section, the theoretical reaction mechanisms of the propene oxide isomerization over H-ZSM-5 zeolite have been presented. Two different products, propanal and propanone, are formed by the breaking of different C-O bonds. The mechanisms start from the ring-opening of propene oxide coordinated to the acidic proton of zeolite to form the intermediate, processing via the carbenium-like ion as the transition state, followed by a 1,2-hydride shift between the adjacent carbon atom to form the carbonyl compounds. With the aim of describing the effect of the zeolite framework on this reaction, the results obtained from the zeolite framework effect are discussed, and are compared with the ones obtained from the active site. In the Results and Discussion section, the details of the energetics and structural stabilities affected from the zeolite framework are also related.

In addition to zeolites, carbon nanotubes (CNTs) are also important nanostructured materials. They are an allotrope of carbon and are generally considered to belong to the fullerene family (Figure 6). The structure of carbon nanotubes can be imagined as a layer of graphite sheet (a hexagonal lattice of carbon) rolled up into a cylinder such that the lattice of carbon atoms remains continuous around the circumference. The number of shells varies from one (a single-walled carbon nanotube) to many with the spacing between the layers matching closely the layer spacing in graphite, around 3.4 Å. CNTs are usually 10-500 Å in diameter and typically a few microns long, although multi-walled nanotubes as long as 200 Å have been grown.

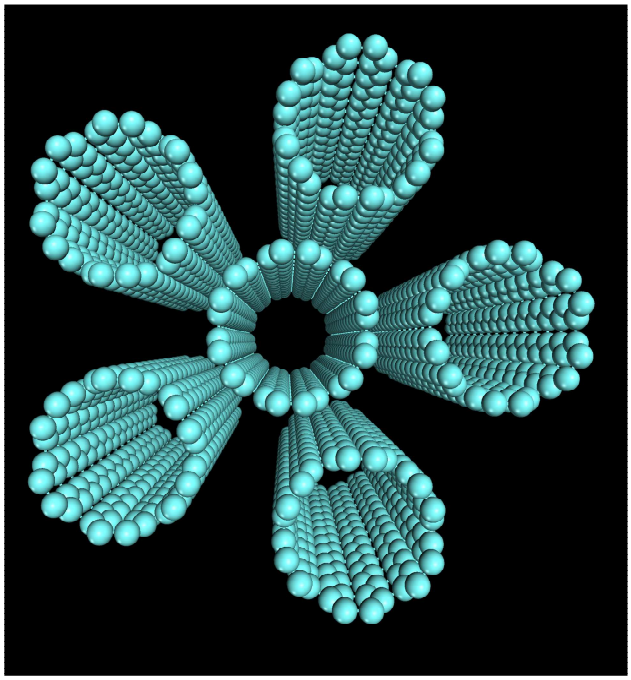

a)

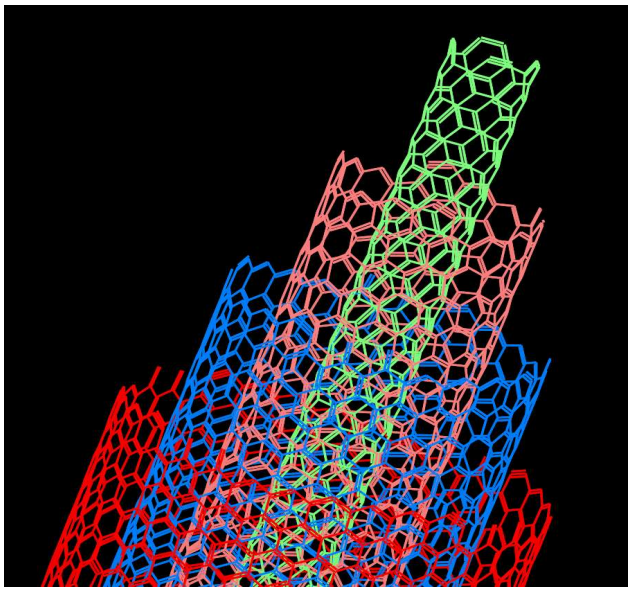

b)

Figure 6 a) Single-walled carbon nanotube (SWNT) bundle and b) Multi-walled carbon nanotubes (MWNTs).

Apart from applied pressure, force etc., defects also affect the basic properties of CNTs. There are three types of defects: topological, rehybridization and incomplete bonding in carbon nanotubes. The most important topological “Stone-wales” defect is a combination of two pentagons and two heptagons (5-7-7-5 defect). This kind of defect causes little change to the diameter and chirality of the CNT and the deformation effect is rather local. And, this transformation effectively elongates the tube in the strain direction, releasing the excess strain energy. This defect can be incorporated in a normal tube by a 90° rotation of the C=C bond between two hexagons. This rotation changes four neighboring hexagons into two pentagons and two heptagons as shown in Figure 7.

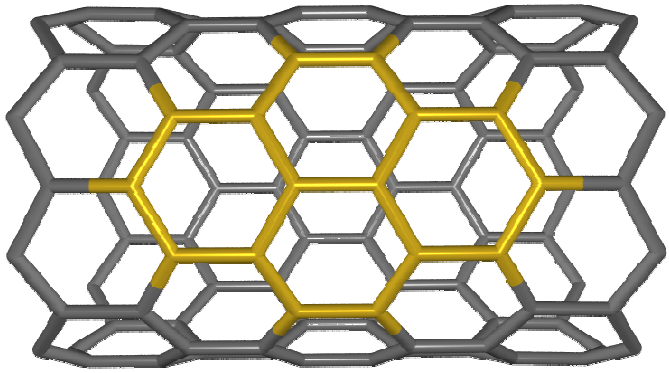

a)

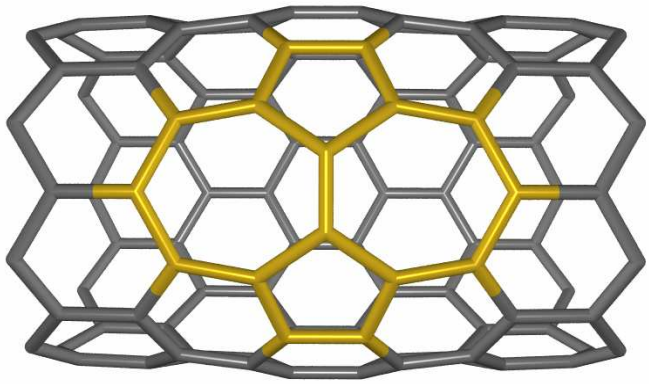

b)

Figure 7. Zigzag (9,0) CNT with a) Perfect and b) Stone-Wales defect (indicated in yellow color).

Nitrous oxide (N_2O) is a toxic pollutant gas in the atmosphere, which often occurs during the incomplete combustion of fossil fuel. The major sources of N_2O gas emission are chemical processes related to the production and utilization of nitric acid as fluidized bed combustion. Their contribution is about 20% of the total exhausted N_2O gas (Kapteijn *et al.,* 1996). Responsible members of the public and industrialists are committing themselves to reduce greenhouse gases by at least 5–8% by the year 2012 (Christoforou *et al.,* 2002). Therefore, the removal of N_2O is definitely a challenging issue.

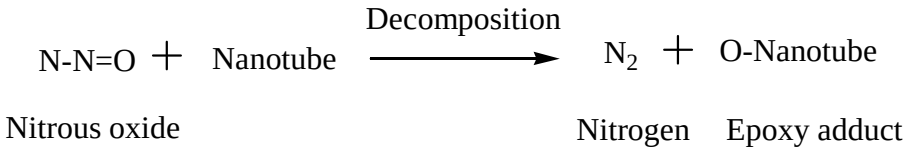

Figure 8. Decomposition of nitrous oxide (N_2O) over nanotube to nitrogen molecule (N_2) and epoxy-adduct.

Carbon nanotubes, especially single-walled carbon nanotubes (SWNTs), have attracted much attention for their fascinating structural, mechanical, electrical, and electromechanical properties (Avouris 2002, Dekker 1999, Ouyang *et al.,* 2002). These nano-structural materials can be modified by functionalization on the open ends or on the sidewall with organic or inorganic compounds to develop many interesting alternative applications. The decomposition of N_2O over SWNTs may be another way of functionalization as this process is not only producing an epoxy adduct of SWNTs for further utilizations, but also converting a toxic N_2O to a nontoxic N_2 molecule. Therefore, in the catalytic aspect, the SWNTs might be a novel and excellent choice of catalyst for the nitrous oxide decomposition due to their high surface area and large number of active sites. In this aspect, the epoxy-adduct, which is considered as a deactivated complex, can be reactivated easily by photodesorption of the oxygen to clean the SWNTs (Miyamoto *et al.,* 2004, Shim *et al.,* 2005, Zhou *et al.,* 2003). Hence, the understanding of the decomposition of N_2O to an N_2 reaction mechanism over SWNTs is useful as the basis for other catalytic applications.

This part of the thesis work reports the first attempt to study this idea to see if there is any possibility to use nanotubes for the removal of toxic gas. In this study, we used the armchair (5,5)-SWNTs as a catalyst for nitrous oxide decomposition and predicted their reaction mechanisms. The roles of the Stone-Wales defect and the presence of a chloride anion inside the armchair (5,5)-SWNTs are also taken into consideration. These results would assist the experimentalists in selecting an effective condition for further explorations.

LITERATURE REVIEW

In catalytic application, zeolites are widely used in the petroleum and petrochemical industries for a number of commercially important hydrocarbon reactions due to their outstanding properties, i.e., Brønsted and Lewis acid sites, size-shape selectivity, and thermal stability. Using proton- and metal-zeolites as the catalysts can increase the percentage yield of the required products and thus reduce the production cost significantly. Zeolites were used as effective catalysts in converting many hydrocarbon materials to value-added products. Several types of zeolites were reported to have high activity for benzene alkylation, for example, faujasite, beta, H-ZSM-5, and MCM-22 (Becker *et al.*, 1973, Chen *et al.*, 1986, Corma 1995, Corma *et al.*, 2000, Degnan Jr *et al.*, 2001, Kaeding *et al.*, 1988, Morita *et al.*, 1973, Reddy *et al.*, 1993, Smirniotis *et al.*, 1995, Venuto *et al.*, 1966, Weitkamp 1985).

The structures of zeolites are microporous aluminosilicates with a large number of atoms in the unit cell. To obtain more manageable sizes for the ab initio calculations, small clusters representing the catalytic active site were studied in the past (Correa *et al.*, 2002, Evleth *et al.*, 1996, Vos *et al.*, 2001, Vos *et al.*, 2003). However, this was meant that the essential confinement effect created by the part of the surrounding framework was neglected. In earlier theoretical studies (Vos *et al.*, 2003), it was deemed sufficient to investigate only the reaction mechanisms of small clusters using first-principle calculations on the reactions of small- and medium-size adsorbates. However, those clusters precluded consideration of the electrostatic and van der Waals effects of the zeolite framework, which significantly affect the stability of the intermediates and transition states. It is important, therefore, that the larger clusters which include such potential be taken into consideration. To facilitate this, the large quantum clusters and periodic calculations were specifically developed.

However, even though these calculations do provide accurate results, they are really prohibitive in terms of computational time and expense. The more recent development of hybrid methods, such as the embedded cluster or combined quantum

mechanics/molecular mechanics (QM/MM) (Braendle *et al.,* 1998, Greatbanks *et al.,* 1996, Hillier 1999, Khaliullin *et al.,* 2001, Limtrakul *et al.,* 2000, Treesukol *et al.,* 2001) was successfully used to model structure and reactivity of zeolites (Braendle *et al.,* 1998, Greatbanks *et al.,* 1996, Hillier 1999, Khaliullin *et al.,* 2001, Limtrakul *et al.,* 2000, Treesukol *et al.,* 2001). An embedded cluster model represented the interaction of substrates with the Brønsted acid site of zeolites was described which utilizes an electrostatic field obtained from calculations of the full periodic structure. Ferthermore, embedded cluster QM/MM calculation at the DFT/MM level was performed to investigate cyclization of C_6 diene leading to C_6 cyclic product in HZSM-5 by comparison to quantum cluster calculation (Joshi *et al.,* 2005). It was shown to be essential for proper analysis of C_6 olefin chemistry in ZSM-5 models with fairly important distinctions between QM/MM and quantum cluster results.

Besides that another development method, the ONIOM (our own n-layered integrated molecular orbital and molecular mechanics), were also made it possible to successfully describe the confinement effect from the zeolite wall as well and at a much more economical computational cost (Dapprich *et al.*, 1999, Solans-Monfort *et al.,* 2002, Svensson *et al.,* 1996). This approach was proposed and shown to be successful in reproducing benchmark calculations and experimental results (Kasuriya *et al.,* 2003, Namuangruk *et al.,* 2004, 2005, 2006). ONIOM3, a three-layered version, divides a system into an active part treated at a very high level of ab initio molecular orbital theory, a semi active part that includes important electronic contributions and is treated at the HF or MP2 level, and a non active part that is handled using force field approaches.

The structure and properties of active intermediates of acid-catalyzed homogeneous and heterogeneous transformations of olefins and alcohols, taking into account the hydration in homogeneous systems or the interaction with the surface of heterogeneous zeolite catalysts on the basis of nonempirical quantum-chemical calculations is discussed by Kazansky *et al.* (1992). In both cases carbenium ions do not represent the actual existing active intermediates, but rather the excited transition states. They could be formed from the more covalent and more stable surface esters in

heterogeneous acid catalysis or from hydrated alkoxonium ions in acid catalysis in aqueous solutions. These results in concerted reaction pathways with low activation energies due to almost complete compensation of the energy required for the rupture of the reacting chemical bonds in the initial compounds by the energy released by the formation of the new bonds in the final products. Seven year later, Kazansky (1999) additionally discussed that adsorbed carbenium ion-like activated complexes can be formed both via proton additional to the double bonds of olefins or as energetically excited unstable ion pairs resulting from partial dissociation of the carbonyl bonds in more stable alkoxy species. In contrast, the highly energetically excited adsorbed carbonium ion-like transition states result only from proton attack at the C-C or C-H bonds of paraffins. The quantum chemical calculations provided the information on geometry and electronic structure of these activated complexes which depend on the elementary reactions in which these transition states are involved. The calculated heat effects and activation energies for main elementary steps in acid catalyzed transformations of hydrocarbons on zeolites, i.e. of double bond shift, skeletal isomerization and cracking of olefins or protolytic dehydrogenation, protolytic cracking of paraffins and hydride transfer from isoparaffins to carbenium ions are in a reasonable agreement with the experiment.

The experimental work of Cant and Hall (1972) showed the activation energy for deuterium exchange of ethylene on H-faujasite of 16 kcal/mol with an adsorption energy of the order 9 kcal/mol. The experimental determination of adsorption of both acetylene and ethylene on a H-ZSM-5 by Haw and co-workers (1989) mentioned that deuterium isotope exchange with ethylene occurs within several hours at room temperature. However, exchange with acetylene takes several days. The adsorption enthalpy can be bracketed between -5 and -10 kcal/mol, which is in qualitative agreement with the work of Cant and Hall. It is also found that acetylene on H-ZSM-5 is unreactive at room temperature but becomes reactive above 425 K. All these works imply that activation energies for isotope exchange of ethylene are lower than for acetylene. These probably range between 15 and 20 kcal/mol for former and between 20 and 25 kcal/mol for the latter.

Ab initio molecular-orbital calculations using the 3-21G basis set is used to study the protonation reaction of propylene and isobutene by zeolite bridged hydroxyls ZOH, which are simulated by a cluster model which consists of two Si tetrahedra and one A1 tetrahedron are studied by Viruela-Martin (1993). The calculations show that in all reactions the adsorption of the olefin molecule on the acidic OH group takes place, leading to a stable π-complex with a structure similar to those of the isolated olefin and clusters constituents. The π-complex is transformed into a zeolite-alkoxide of covalent characteristics. The surface alkoxides are the most stable structures with reaction energies in the range of -15 to -7 kcal/mol. These reactions take place through transition states whose organic fragment has a geometry and charge distribution resembling those of the 2-propyl and *tert*-butyl classical carbenium ions for zeolite-propylene and -isobutene, respectively. The obtained activation energies (30-40 kcal/mol) are of the same order of magnitude in all the reactions considered. The bifunctional mechanism of the reactions is rather complicated and implies a concerted process involving the proton transfer from the zeolite toward a carbon of the olefin double bond, and the simultaneous C-O bond formation at the adjacent oxygen on the zeolite structure. The reaction mechanism and the properties of the transition states are practically the same. It is then proposed that the geometric conformation of transition state can be more determinant than the chemical composition of the zeolite. In this respect, the flexibility of the zeolite structure plays an important role.

Later, Beck and co-worker (1995) used Density Functional Theory (DFT) calculations on a cluster model to investigate the H/D–exchage of benzene, the most simple electrophillic aromatic substitution reaction. They compared the catalytic performance of β-zeolite in the liquid-phase alkylation of benzene with that of other solid catalysts. β-zeolite is more active and more selective than faujasite zeolite in the alkylation with propylene and ethylene to cumene and ethylbenzene (EB). In the alkylation with propylene the overall selectivity of β-zeolite is higher than that of the traditional “solid phosphoric acid”. The catalytic activity is affected by the composition and the particle size of β-zeolite samples. The catalytic activity of β-

zeolite is limited by intraparticle diffusion, as evidenced by the decreased activity corresponding to the particle size increase.

Ab initio quantum chemical methods are used to study the mechanisms for the hydrocarbon conversion in zeolites, i.e. cracking, isomerization, alkylation, etc. (Rigby *et al.*, 1997). It is found that the intermediates are covalent alkoxide species and indicate that there is no energy ordering of these alkoxides according to their primary, secondary, or tertiary nature. Transition states have been located for the most important conversion reaction steps for hydrocarbons up to C_6. The reactions are concerted and the transition states are ionic and ring-like. Due to charge delocalization in the transition state the activation energies depend on the nature of the initial and final alkoxides. These calculations are the foundation for a new model of the hydrocarbon conversion which can better describe the influence of the zeolite as will be illustrated with calculations on acid sites with varying acid strength.

The density functional theory is used to study the mechanism of double-bond isomerization and skeletal isomerization of linear butanes catalyzed by a protonated zeolite, which is simulated by a cluster consisting of two Si and one Al tetrahedral (Boronat *et al.*, 1998). The study includes complete geometry optimization and characterization of reactants, products, reaction intermediates and transition stated, and calculation of the activation energies for the different processes involved. It is shown that the double bond isomerization proceeds by a concerted mechanism which does not involved the formation of either ionic or covalent alkoxy intermediates. According to this concerted mechanism, in one step the acid OH group of the zeolite protonates the double bond of adsorbed but-1-ene and the basic neighboring O atom of the cluster abstracts hydrogen from the olefin, restoring the zeolite active site and yielding adsorbed but-2-ene. However, the mechanism of skeletal isomerization of linear butanes consists of three elementary steps: protonation of adsorbed primary a secondary alkoxy intermediate, conversion state in which the transferring methyl group is halfway between its position in the linear and in the branched species, and decomposition of the primary alkoxy intermediate to give adsorbed isobutene. The

activation barriers calculated for the two reactions are in good agreement with experimental data.

The results obtained from quantum chemical calculations using density functional theory and Hartree-Fock methods indicate that the potential energy surface for the mechanism of the β-scission reaction in zeolites is very complex (Frash *et al*., 1998). Three reaction paths were identified: (i) path RL, one-step via the "ringlike" transition state (TS); (ii) path HBCP, via the "hydrogen-bonded" TS and substituted cyclopropane; and (iii) path HB, one-step via the "hydrogen-bonded" TS. Transition states in all reaction paths represent complexes of the carbocation-like fragment with the negatively charged cluster, whereas both initial and final states represent alkoxy species with a covalent bond between a carbon atom of the hydrocarbon portion and a zeolite oxygen. The B3LYP/6-31++G**//B3LYP/6-31G* activation energies for β-scission of but-1-oxy and pent-2-oxy with the $H_3Si(OH)AlH_2(OSiH_3)$ cluster were found to be 57.4 and 52.4 kcal/mol, respectively.

It is found that MCM-22, beta, and USY zeolite exhibited very different behavior in the liquid-phase alkylation of benzene with ethylene (Cheng *et al.*, 1999). MCM-22 zeolite was the most selective for ethylbenzene synthesis, with by product of < 0.07% wt. even at near-complete ethylene conversions. Zeolite beta was the most active (e.g. approximated 3 times higher for MCM-22 and much higher than for high-activity USY zeolite), but it produced significantly higher levels of heavy byproducts (i.e., butylbenzenes and diphenylethanes). USY aged rapidly and had relatively poor selectivity for ethylbenzene. The USY zeolite had a much higher selectivity for oligomerization than the other two zeolites, presumably because it had a larger pore structure that allowed the formation of bulkier polyalkylated benzenes. Also, Corma and co-worker (2000) studied benzene alkylation with ethylene and propene which has been carried out under liquid-phase reaction conditions over zeolites MCM-22, Beta, and ZSM-5. They found that MCM-22 seems to be a good catalyst for benzene alkylation especially with propene, showing high activity and stability and good selectivity. Beside that, they developed a mechanistic model for the alkylation of benzene with propene in order to achieve not only a kinetic expression useful for

reactor design but also a better understanding of the molecular events occurring during alkylation on zeolite MCM-22. Their results showed that kinetic experiments of alkylation with propene followed an Eley-Rideal type mechanism. Beside that, they fitted the experimental values to the Arrhenius equation, and an activation energy of 18.4 kcal/mol has been obtained. Another value of 10 kcal/mol over an HM zeolite, 17.9 kcal/mol over Fe-FMI zeolites and 12-16 kcal/mol for CaY and LaY zeolites have been reported for benzene isopropylation to cumene.

An overview of current industrial alkylation processes for the production of ethylbenzene and cumene are provided by Degnan Jr. and co-worker (2001). Zeolite catalysts have begun to displace the conventional aluminum chloride and solid phosphoric acid (SPA). Friedel-Crafts catalysts used in both ethylbenzene and cumene processes. This transformation has been particularly rapid in the case of ethylbenzene and cumene technology. Kato *et al.* (2001) carried out the alkylation of benzene with ethane and ethylene by using various zeolite catalysts such as H-Y, H-ZSM-H, H-mordenite at temperature ranges of 400-500 °C. Among the zeolites tested, H-ZSM-5 and H-MCM-22 showed catalytic activities. Loading of platinum onto zeolite greatly enhanced the yield of ethylbenzene. In the alkylation of benzene with ethane over platinum-loaded H-ZSM-5, ethylene was initially formed from ethane over the metallic platinum. Then the alkylation proceeded over the acid site of H-ZSM-5.

The alkylation of benzene with ethylene over β-zeolite catalyst to ethylbenzene has been studied by in situ IR (Du *et al*., 2002). The proposed mechanism is follows: adsorbed ethylene on weaker acidic site may react with adsorbed benzene or ethylbenzene on strong acidic sites. These substances are adsorbed competitively at the same kind of sites. Ethylene adsorbed becomes carbenium, a substance which has strong interaction with acidic sites, on the other hand, benzene and ethylbenzene adsorbed molecularly have weak interaction, in the form of hydrogen bonding, with acidic OH.

Vos and co-worker (2001) reported the theoretical study of the alkylation of toluene with methanol catalyzed by the acidic Mordenite (Si/Al=23). They showed how steric constraints in zeolites affect reactivity. Their results showed that transition state selectivity is included within mordenite. Quantitatively, this selectivity can be estimated by the comparison of the activation energies: the activation energy differences are of the order of 5 kcal/mol. The order of the activation energies of xylene change completely when the activation energies are considered in the presence and absence of steric constraints. In the absence of steric constraints the order is ortho < para < meta, in good agreement with the HSAB principle, whereas in the presence of steric constraints. In the absence of steric constraints this becomes para < ortho < meta. These activation energy differences are not sufficient to explain the 100% selectivity. These modified zeolite catalysts have been pre-coked and their external active sites have been deactivated. Diffusional processes may then play an important role.

A periodic density functional theory (DFT) study of the isomerization reaction of toluene and xylene catalyzed by acidic mordenite was reported by Rozanska *et al.* (2001). They have shown how a combination of steric constraints and electrostatic contributions of zeolitic atoms can affect the reaction pathways of intramolecular isomerization reaction of toluene and xylene isomers. Isomerization reactions may proceed according to different reaction pathways which do not show energetic differences in the absence of steric constraints. It has been observed that zeolitic channel oxygen atoms play an important role on the stabilization of the transition states. The location of the transition states with respect to the Brønsted site can be altered completely if the zeolitic topology allows a more efficient way to stabilize the transient species. Apart from this, the reaction mechanisms obtained via the cluster approach and periodic calculation remains, in essence, similar. Small cluster calculations have been proven to give good qualitative results compared with periodic results. Differenced results from the fact that zeolitic micropore oxygen atoms are not passive spectators but rather participate actively in the catalysis of reactions. The contribution of the zeolitic oxygen atoms appears to be of short-range nature. The presence of steric constraints has been shown to inhibit the possibility that

isomerization of toluene and xylene proceed via some reaction pathways. Destabilization of transition states is up to 12 kcal/mol although aromatics can fit without difficulty inside the mordenite large pores. Steric constraints are strongly dependent on the transition-state structure as well as son the zeolite topology.

To study the effects related to long-range interactions between the reaction site and its environment. The ONIOM method is a generalized hybrid scheme to treat different levels of theory. Its implementation in the Gaussian program system allows the definition of up to three arbitrarily shaped layers with the free choice of the method for every part. All methods available in Gaussian can be used without any modification of the parametrization. For the situation where covalent bonds need to be cut in order to generate a model system, an improved link atom technique is employed. Besides energy calculations, ONIOM allows geometry optimizations, vibrational frequency calculations, and the evaluation of electric field derivatives such as dipole moments, polarizabilities, hyperpolarizabilities, IR intensities, and Raman intensities. Dapprich *et al.* (1999) describes the unification, generalization, and extension of their recently introduced IMOMM, IMOMO and ONIOM (Svensson *et al.*, 1996) methods that have been proven to be very valuable and promising tools for the treatment of large molecular system. In contrast to other hybrid methods, ONIOM treats the interaction between the model and the real system consistently at a well defined level of theory. Due to the virtually free choice of method combinations and system partitioning, ONIOM is scalable and can be systematically improved. This allows its successful and reliable application to a wide variety of chemically interesting problems.

Sillar and co-worker (2002) tested the performance of the ONIOM method on reproducing the properties of the acid sites of the zeolite ZSM-5. The acid sites in three crystallographic locations have been modeled by three combinations of two-layer ONIOM method with varied size (two and eight tetrahedral, T, atoms) and calculation method (ab initio and DFT) used for the chemically important (active) part. The best correspondence with experimental data was achieved calculated with ONIOM(B3LYP/6-311+G(d,p):MNDO) method using eight T atoms in model system

for the following properties: stretching vibrational frequencies, ^{1}H NMR chemical shifts of the bridged hydroxyl group, vibrational frequency shifts and changes in 1H NMR chemical shifts of the hydroxyl groups upon adsorption of CO.

The keto-enol isomerization of acetaldehyde inside H-ZSM5 was investigated using the B3LYP density functional approach and modeling the zeolite with T3 and T5 clusters (Solan-Monfort *et al.*, 2002). Moreover, the effect of enlarging the cluster to T63 has been considered using the ONIOM2 approach and combining the B3LYP method with the AM1 or MNDO semiempirical ones. It was observed that the zeolite produces an important catalytic effect on the enolization reaction. The catalytic effect was much larger than that produced by a water molecule, due to the larger acidity of the zeolite and to smaller geometry reorganizations along the process. Calculations with all clusters indicated that the adsorption of acetaldehyde to zeolite corresponded to a neutral complex and not to an ion pair. Results with cluster T3 and T5 are very similar. Enlarging the size of the cluster to 63 tetrahedra with the ONIOM2 approach destabilizes the keto intermediate and stabilizes the enol one, which results in a decrease of the endothermicity of the reaction. The computed energy barrier and reaction energy of the HZ (keto) to HZ (enol) reaction at the ONIOM2(B3LYP:AM1) level are 18.0 and 7.4 kcal/mol, respectively. The ONIOM2 procedure was considered quite large clusters at a reasonable computational cost, which naturally introduce the limited flexibility of the zeolite without imposing artificial constraints.

For the dimerization of ethylene, the reaction was considered to proceed by the protonation of the alkene molecule by the Brønsted acid site of the zeolite to give a carbenium cation which subsequently reacted with another alkene molecule to form a dimer complex. Recently, Zecchina group (Geobaldo *et al.*, 1997, Spoto *et al.*, 1994) studied oligomerization of ethylene and propylene on H-mordenite using FTIR spectroscopy and reported that the reactions proceed in a stepwise manner. The reactions start with the protonation of adsorbed alkenes and then chain propagation by insertion of monomeric alkenes. Svelle *et al.,* (Svelle *et al.,* 2004) theoretically investigated the dimerization of linear alkenes (ethylene, propylene, and butene) by acidic zeolite and suggested that in addition to the stepwise mechanism, the concerted

mechanism should also be considered. Theoretical studies can offer a practical means to elucidate the reaction mechanism at the molecular level and support and/or guide experimental investigations.

The ring-opening reactions of propene oxide on various zeolites and zeotypes (HZSM-5, CuZSM-5, HY, AlMCM-41, SiMCM-41, and BMCM-41) were investigated in the presence of hydrogen or nitrogen (Fasi *et al.*, 2001). The acidic molecular sieves were found to be active in isomerization (the products are propanal and propanone) and dimerization (the products are dioxolane and dioxane derivatives) reactions. Numerous experimental and theoretical studies have investigated the reactions and mechanisms of the ring-opening isomerization, the isomerization of epoxides in solutions with and without acid catalysts and catalytic enzymes (Carlier *et al.*, 2006, Coxon *et al.*, 1997, Dimitrova *et al.*, 1996, Fasi *et al.*, 2001, Fasi *et al.*, 2004, George *et al.*, 1992, Helten *et al.*, 2004, 2005, Lau *et al.*, 2001)

A number of previous studies were addressed the structure of protonated epoxides and their energies relative to the corresponding ring-opened hydroxy-carbocations (Coxon *et al.*, 1997, George *et al.*, 1992, Lau *et al.*, 2001). The acid- and BF_3-catalyzed rearrangement of propene oxide to propanal was investigated by density functional methods (Coxon *et al.*, 1999). Isotope effects were calculated and were consistent with the reaction occurring via a carbocation intermediate followed by a 1,2-hydride shift. Inverse secondary isotope effects for hydride migration reflect a combination of changes in C1-H(D) stretching and out-of-plane bending frequencies with a stronger force constant of the nonmigrating C1-H bond at the transition structure than in the carbocation.

Recently, there have been several theoretical and experimental investigations which modify the sidewall of SWNTs by undergoing the 1,3-dipolar cycloaddition (Georgakilas *et al.*, 2002, Lu *et al.*, 2003a, Tagmatarchis *et al.*, 2004), [2+1] cycloaddition (Chu *et al.*, 2004, Holzinger *et al.*, 2004, Hu *et al.*, 2003, Li *et al.*, 2002, Lu *et al.*, 2005, Lu *et al.*, 2003b, Su 2005), fluorination (Kawasaki *et al.*, 2004, Lebedev *et al.*, 2003, Nakajima *et al.*, 1996), Diels-Alder cycloaddition (Delgado *et*

al., 2004, Lu *et al.*, 2002a, Warakulwit *et al.*, 2005, Zhang *et al.*, 2005), ozonolysis (Liu *et al.*, 2006, Lu *et al.*, 2002b, Picozzi *et al.*, 2004, Yim *et al.*, 2004), and hydroboration (Long *et al.*, 2003) in order to introduce new physical and chemical properties.

There are theoretical studies on the relationship of the chemical reactivities of the sidewall of (5,5) carbon nanotubes and the length of finite clusters (Bettinger 2004, Matsuo *et al.*, 2003). From the nuclear independent chemical shift (NICS) analysis and molecular orbital studies, Matsuo and co-worker (Matsuo *et al.*, 2003) demonstrated that the chemical and electronic structures of carbon nanotubes oscillate as the tube was elongated from $C_{40}H_{20}$ to $C_{200}H_{20}$ generating Kekule', incomplete Clar and complete Clar networks in the periodicity of three. Without any indication of chemical modification, the author suggested that the complete Clar network in the series of $C_{60}H_{20}$, $C_{90}H_{20}$, $C_{120}H_{20}$, etc., having the smallest band gap should have the highest chemical reactivity. Afterward, Bettinger (Bettinger 2004), studied the carbene addition to the sidewall of the (5,5) armchair tube at the 1,2-pair site using finite clusters of various lengths. They concluded that the minimal model for studying the chemistry of the (5,5) armchair nanotubes should be the $C_{90}H_{20}$ model in which the effects from the edges in calculations are neglectable.

Ozonization of the sidewalls of single-wall carbon nanotubes has been investigated by means of 2-layered ONIOM(B3LYP/6-31G*:AM1) calculations (Lu *et al*., 2002c). The theoretical calculations reveal that the 1,3-dipolar cycloaddition (1,3-DC) of ozone (O_3) onto the sidewalls of a (5,5) carbon nanotube is site-selective and facile with a small activation barrier of 1.4 kcal/mol. The desorption of ozone from the thus-formed ozonide was found to be favorable over the decomposition process that gives rise to epoxy adduct and O_2 upon thermal activation. This work implies the possibility of functionalizing the sidewalls of SWNTs by means of 1,3-dipolar cycloadditions of 1,3-dipolar molecules.

A Stone–Wales defect in CNTs is a dipole of 5–7 ring pair in a hexagonal network, which is one of the most important defective structures in CNTs that will

affect mechanical, chemical, and electronic properties of CNTs. Using the extended Hückel method, Zhou and co-worker (2003) calculated the formation energy of SW defects in carbon nanotubes. The formation energy of Stone–Wales defects was then fitted to a simple formula as a function of the tube radius and the orientations of a SW defect in the tube. The mechanism of Stone-Wales transformation is studied by means of the hybrid density functional method (Jin *et al.*, 2005). The results showed that the transition of the D_{6h} neutral and charged isomers to D_{2d} isomers of C_{36} and reaction pathway could be identified for the rearrangement from C_{36}-D_{6h} to C_{36}-D_{2d} on the potential energy surface. It is found that the neutral and charged transition states all have C_2 molecular point group symmetry with the two migrating carbon atoms remaining close to the fullerene surface. The other kind of possible TS with a carbene-like structure along the stepwise reaction path does not exist as a stationary point with the density functionals utilized here. The classical barriers are 143.7 kcal/mol through the neutral TS, 155.3 kcal/mol through the anionic TS, and 145.1 kcal/mol through the cationic TS at the B3LYP/6-31G level of theory.

Wang *et al.* (2006) investigated the chemical functionalization of carbon nanotubes with Stone-Wales defects by carboxyl (COOH) groups by density functional calculations. Due to the localized donor states induced by the SW defect, the binding of the COOH group with the defective carbon nanotube was stronger than that with the perfect one. A quasi-tetrahedral bonding configuration of carbon atoms, indicating sp^3 hybrid bonding, was formed in the adsorption site. The charge distribution analysis shows that, in comparison with benzoic acid, the localized or delocalized π-states on the nanotube would affect the polarities of chemical bonds of the COOH group without losing the acidity. Furthermore, it was found that the double-adsorption system (two COOH groups were respectively adsorbed on two individual carbon atoms of the SW defect) was more energetically favorable than the mono-adsorption one. The adsorption of COOH groups leads to a significant change of the electronic states around the Fermi level, which is advantageous for the electrical conductivity. The functionalization by introducing functional groups on the topological defects provided a pathway for applications of carbon nanotubes in chemical sensors and nano-bioelectronics.

The expectation that Stone-Wales defects (5/7/7/5) are more highly reactive than pristine tube walls was confirmed for the reaction with methylene by Bettinger (2005). However, it is also important to realize that significant differences among the addition sites newly generated by the Stone-Wales transformation exist: while some of the bonds show higher reactivity than those in the pristine tubes, others are less reactive. The density functional theory has been performed in order to investigate ozone adsorption on carbon nanotubes (Picozzi *et al*., 2004). Particular emphasis was placed on the effects of Stone–Wales defects on the structural and electronic properties of (i) ideal tubes and (ii) tubes in the presence of ozone. The results showed that structural deformations induced on the pure carbon nanotubes by Stone–Wales defects were similar, as expected, to those induced on graphite; for the (10,0) tube, the semi-conducting character was kept, though with a small reduction of the band gap. As for the ozone adsorption, the process on ideal nanotubes was most likely physisorption, though slightly stronger if compared to other previously studied molecules and consistent with the strong oxidizing nature of ozone. However, when ozone adsorbs on Stone–Wales defects, a strong chemisorption occured, leading to relevant structural relaxations and to the formation of a CO covalent bond; this is consistent with experimental observations of CO functional groups, as well as of the liberation of CO gas phase and of the formation of C vacancies, thus explaining the consumption of the nanotube film upon ozone exposure.

METHODS OF CALCULATIONS

This thesis project used two types of methods in calculations: molecular mechanics and quantum mechanics. The quantum mechanics methods include semi-empirical, ab initio, and density functional methods. The molecular mechanics and semi-empirical methods have several advantages over ab nitio and density functional methods. Most importantly, these methods are fast. While this may not be important for small molecules, it is certainly important for large molecules. Another advantage is that for specific and well-parameterized molecular systems, these methods can calculate values that are closer to experiment than lower level ab initio and density functional techniques.

The accuracy of a molecular mechanics or semi-empirical quantum mechanics method depends on the database used to parameterize the method. This is true for the type of molecules and the physical and chemical data in the database. Frequently, these methods give the best results for a limited class of molecules or phenomena. A disadvantage of these methods is that one must have parameters available before running a calculation. Developing parameters is time-consuming.

The ab initio or density functional methods may overcome this problem. However they are slower than any molecular mechanics and semi-empirical methods.

1. Molecular Mechanics

Molecular mechanical force fields use the equations of classical mechanics to describe the potential energy surfaces (PES) and physical properties of molecules. A molecule is described as a collection of atoms that interact with each other by simple analytical functions. This description is called a force field. One component of a force field is the energy arising from compression and stretching a bond. This component is often approximated as a harmonic oscillator and can be calculated using Hooke’s law;

$$V_{spring} = \frac{1}{2} K_r (r - r_0)^2 \quad (1)$$

The bonding between two atoms is analogous to a spring connecting two masses. Using this analogy, V_{spring}, and the force constant of the spring, K_r. The equilibrium and displaced distances of the atoms in a bond are r_0 and r. Both K_r and r_0 are constants for a specific pair of atoms connected by a certain spring. K_r and r_0 are force field parameters.

The potential energy of a molecular system in a force field is the sum of individual components of the potential, such as bond, angle, and van der Waals potentials. The energies of the individual bonding components (bonds, angles, and dihedrals) are functions of the deviation of a molecule from a hypothetical compound that has bonded interactions at minimum values.

$$E_{Total} = term_1 + term_2 + ... + term_n \quad (2)$$

The absolute energy of a molecule in molecular mechanics has no intrinsic physical meaning; E_{Total} values are useful only for comparisons between molecules. Energies from single point calculations are related to the enthalpies of the molecules. However, they are not enthalpies because thermal motion and temperature dependent contributions are absent from the energy terms.

Unlike quantum mechanics, molecular mechanics does not treat electrons explicitly. Molecular mechanics calculations cannot describe bond formation, bond breaking, or systems in which electronic delocalization or molecular orbital interactions play a major role in determining geometry or properties.

2. Quantum Mechanics

2.1 Semi-empirical Method

Semi-empirical methods are techniques which use approximations from empirical (experimental) data to provide the input into the mathematical models. These methods lie between ab initio and molecular mechanics (MM). Like MM, they use experimentally derived parameters to attempt for accuracy; like ab initio methods, they are quantum-mechanical in nature. The semi-empirical methods used in this thesis project are listed below.

2.1.1 MNDO

MNDO is a Modified Neglect of Diatomic Overlap method based on the neglect of diatomic differential overlap (NDDO) approximation. The method was proposed and developed by M. J. S. Dewar and co-workers at the University of Texas at Austin (Dewar *et al*. 1977, 1978). The elements of the MNDO Fock matrix based on the neglect of diatomic differential overlap approximation are described below.
When φ_μ and φ_ν are on different centers the off-diagonal elements of the Fock matrix are:

$$F_{\mu\nu}^{\alpha} = H_{\mu\nu} - \sum_{\lambda}^{A}\sum_{\sigma}^{B} P_{\lambda\sigma}^{\alpha}(\mu\lambda \mid \nu\sigma) \tag{3}$$

(μ on A, ν on B, A≠B)
and when φμ and φν are different atomic orbitals but on the same center then the off-diagonal elements of the Fock matrix are:

$$F_{\mu\nu}^{\alpha} = H_{\mu\nu} + P_{\mu\nu}^{\alpha}[3(\mu\nu \mid \mu\nu) - (\mu\mu \mid \nu\nu)] + \sum_{B}\sum_{\lambda}^{A}\sum_{\sigma}^{B} P_{\lambda\sigma}^{\alpha}(\mu\lambda \mid \nu\sigma) \tag{4}$$

(μ on A, ν on A, $\mu \neq \nu$)
The diagonal elements of the Fock matrix are:

$$F_{\mu\mu}^{\alpha} = H_{\mu\mu} + \sum_{\nu}^{A} P_{\nu\nu}^{\alpha} + \beta_{(\mu\mu|\nu\nu)} + \sum_{B}\sum_{\lambda}^{B}\sum_{\sigma}^{B} P_{\lambda\sigma}^{\alpha}\beta_{(\mu\mu|\lambda\sigma)} \tag{5}$$

where $\mathbf{P}^T = \mathbf{P}^{\alpha+\beta} = \mathbf{P}^\alpha + \mathbf{P}^\beta$. By replacing the superscripts α and β by β and α, respectively, in the above three equations, you can easily get three similar equations for the Fock matrix elements for beta orbitals. Similar expressions to the above for Fock matrix elements of restricted Hartree-Fock (RHF) calculations can be generated by simply replacing $\mathbf{P}^\alpha$ (or $\mathbf{P}^\beta$) by -1/2 $\mathbf{P}^T$ in the above equations.

MNDO has been used widely to calculate heats of formation, molecular geometries, dipole moments, ionization energies, electron affinities, and other properties. It has problems dealing with sterically crowded molecules (too unstable), four-membered rings (too stable), hydrogen bonding (almost nonexistent), and hypervalent compounds (too unstable). Also, nitrobenzene incorrectly yields an out-of-plane nitro group, and the peroxide bond is too short by about 0.17 Å. Although AM1 is generally a significant improvement over MNDO, MNDO gives better results for some classes of molecule, such as some phosphorus compounds.

2.1.2 AM1 and PM3

AM1 (Austin Model 1) is generally the most accurate computational method included among semi-empirical methods and is often the best method for collecting quantitative information. PM3 is functionally similar to AM1, but uses an alternative parameter set. AM1 is a modified MNDO method proposed and developed by M. J. S. Dewar and co-workers (Stewart *et al.*, 1990). PM3, developed by James J.P. Stewart, is a reparameterization of AM1, which is based on the neglect of diatomic differential overlap (NDDO) approximation. NDDO retains all one-center differential overlap terms when Coulomb and exchange integrals are computed. PM3 differs from AM1 only in the values of the parameters.

The parameters for PM3 were derived by comparing a much larger number and wider variety of experimental versus computed molecular properties. Typically, nonbonded interactions are less repulsive in PM3 than in AM1. PM3 is primarily used for organic molecules, but is also parameterized for many main group elements. While MINDO/3 has proved very effective in studies of a wide variety of

hydrocarbons (Dewar *et al*. 1977), problems arise in the case of molecules containing heteroatoms because of the neglect of one-center differential overlap in the INDO approximation on which MINDO/3 based. The problems are avoided in MNDO but at the expense of other. In particular MNDO fails to reproduce hydrogen bonds correctly, gives energies that are too positive for crowded molecules (e.g. neopentane) and too negative for ones containing four-membered rings, and gives activation energies that tend to be too large. Dewar and co-workers found that the reason is because MNDO overestimates the repulsions between atoms at their Van der Waals distance. Hence they modified the core-core repulsion for N-H and O-H interactions to:

$$E_N(A,H) = Z_A Z_H (s_A s_A \mid s_H s_H) x\left(1 + \frac{\exp(-\alpha_H R_{AH})}{R_{AH}} + \exp(-\alpha_H R_{AH})\right) + \left(\frac{Z_A Z_H}{R_{AH}}\right) x\left(\sum_k a_{kA} \exp\left[-b_{kA}(R_{AH} - c_{kA})^2\right] + \sum_k a_{kH} \exp[-b_{kH}(R_{AH} - c_{kH})^2]\right) \quad (6)$$

and for all other interactions to:

$$E_N(A,B) = Z_A Z_B (s_A s_A \mid s_B s_B) x\left(1 + \frac{\exp(-\alpha_A R_{AB})}{R_{AH}} + \exp(-\alpha_B R_{AB})\right) + \left(\frac{Z_A Z_B}{R_{AB}}\right) x\left(\sum_k a_{kA} \exp\left[-b_{kA}(R_{AB} - c_{kA})^2\right] + \sum_k a_{kB} \exp[-b_{kB}(R_{AB} - c_{kB})^2]\right) \quad (7)$$

Comparing the core-core repulsion of the above two equations with those in the MNDO method, it can be seen that the only difference is in the last term. The extra terms in the AM1 core-core repulsion define spherical Gaussian functions. The a, b, and c are adjustable parameters. AM1 has between two and four Gaussian functions per atom.

These are the only differences between the MNDO and AM1 functional form. Dewar's group regenerated AM1 parameters for the elements H, B, C, N, O, F, Al, Si, P, S, Cl, Zn, Ge, Br, and Sn and found that the main gains in AM1 over MNDO were the ability to reproduce hydrogen bonds and the promise of better activation energies for reactions. AM1 does not significantly change the computation time compared with MNDO.

2.2 The Hartree-Fock Theory

To describe the state of a system in quantum mechanics the existence of a function of the coordinates called the wavefunction is postulated. The wavefunction Ψ contains all possible information about a system. The physical meaning of Ψ was given by Max Born that $|\Psi(r)|^2 d\tau$ is the probability of finding the particle in volume $d\tau$ and then $\int_{\infty} |\Psi(r)|^2 d\tau = 1$. Systems of electrons can be described by their wavefunctions which are the solutions of the Schrödinger equation (Szabo and Ostlund, 1996). The non-relativistic time-independent Schrödinger equation has a general form of

$$\hat{H}\Psi = E\Psi \tag{8}$$

where $\hat{H}$ is the Hamiltonian operator for a system, Ψ is the wavefunction, and E is the corresponding energy of the system. The Hamiltonian operator for systems of n electrons and K nuclei is

$$\begin{aligned}\hat{\mathrm{H}} &= -\sum_{i=1}^{n}\frac{1}{2}\nabla_i^2 - \sum_{A=1}^{K}\frac{1}{2M_A}\nabla_A^2 - \sum_{i=1}^{n}\sum_{A=1}^{K}\frac{Z_A}{r_{iA}} + \sum_{i=1}^{n}\sum_{j<i}^{n}\frac{1}{r_{ij}} + \sum_{A=1}^{K}\sum_{B<A}^{K}\frac{Z_A Z_B}{R_{AB}} \\ &= \hat{T}_e + \hat{T}_n + \hat{V}_{ext} + \hat{V}_{ee} + \hat{V}_{nn}\end{aligned} \tag{9}$$

In Eq. (9), the Hamiltonian operator contains the kinetic energy of the electrons T_e and of the nuclei T_n, the Coulomb repulsions among all the molecule's electrons V_{ee}, the Coulomb attractions among the electrons and all of the molecule's nuclei V_{ext}, and the Coulomb repulsions V_{nn} among all of these nuclei. The wavefunction Ψ and energy E are determined by solving the Schrödinger equation (Eq.(8)).

2.2.1 The Born-Oppenheimer Approximation

Since nuclei are much heavier than electrons, they move much slower. To a good approximation, the electrons can adjust themselves almost

simultaneously to any changes in the position of the nuclei. In the Born-Oppenheimer approximation, we consider electrons in a molecule to be moving in the field of fixed nuclei. The electronic wavefunctions thus depend only on the positions but not on the momenta of nuclei. Therefore, the motion of electron can be decoupled from the motion of the nuclei;

$$\Psi(\{r_i\};\{R_A\}) = \psi_{elec}(\{r_i\};\{R_A\})\,\psi_{nucl}(\{R_A\}) \tag{10}$$

Within the BO approximation, the kinetic energy of the nuclei can be neglected and the repulsion between the nuclei can be considered to be constant. The electronic wavefunction ψ_{elec}, which describes the motion of electrons and depends parametrically on the nuclei coordinates, is the solution to a Schrödinger equation involving the electronic Hamiltonian;

$$\hat{H}_{elec}\psi_{elec} = E_{elec}\psi_{elec} \tag{11}$$

The motion of nuclei is described by the nuclear wavefunction ψ_{nucl}, which is the solution to a nuclear Schrödinger equation;

$$\hat{H}_{nucl}\psi_{nucl} = E\,\psi_{nucl} \tag{12}$$

The electronic Hamiltonian operator $\hat{H}_{elec}$ describing the motion of n electrons in the field of K nuclei is

$$\hat{H}_{elec} = -\sum_{i=1}^{n}\frac{1}{2}\nabla_i^2 - \sum_{i=1}^{n}\sum_{A=1}^{K}\frac{Z_A}{r_{iA}} + \sum_{i=1}^{n}\sum_{j<i}^{n}\frac{1}{r_{ij}} \tag{13}$$

and the nuclear Hamiltonian operator $\hat{H}_{nucl}$ is

$$\hat{H}_{nucl} = -\sum_{A=1}^{K}\frac{1}{2M_A}\nabla_A^2 + E_{elec}(\{R_A\}) + \sum_{A=1}^{K}\sum_{B>A}^{K}\frac{Z_A Z_B}{R_{AB}} \tag{14}$$

Henceforth, the electronic problem of Eq. (11) will be concentrated only on the electronic Hamiltonian $\hat{H}$ and the electronic wavefunctions ψ, without subscript "elec" labeled.

In the Hartree Approximation the n-electron wavefunction Ψ^{HP} is simply written as a product of one-electron wavefunctions ϕ_i.

$$\psi^{HP}(x_1, x_2, ...x_n) = \phi_1(x_1), \phi_2(x_2)...\phi_n(x_n) \tag{15}$$

Such a many-electron wavefunction is termed a Hartree product, with electron-one being described by the orbital ϕ_1, electron-two being described by the orbital ϕ_2, etc. Using the Hartree product, the energy is just the sum of the orbital energies ε_i.

$$E = \varepsilon_1 + \varepsilon_2 + \ldots + \varepsilon_n \tag{16}$$

The orbital energies ε_i are obtained from

$$h(i)\phi_j(x) = \varepsilon_j \phi_j(x) \tag{17}$$

where $h(i)$ is the operator describing the kinetic energy and potential energy of electron i.

The Hartree product is an uncorrelated wavefunction because the probability of finding one electron at a given point in space, $|\phi_i(x_i)|^2 dx_i$, is independent of the position of other electrons. Moreover, it takes no account of the indistinguishability of electrons.

2.2.2 The Slater Determinant

To satisfy the Pauli Exclusion principle – that the wavefunction of electrons must be antisymmetric with respect to electron-interchange, in the Hartree-Fock theory the wavefunction is given by the Slater determinants of N spin-orbitals.

$$\psi(x_1, x_2, ...x_n) = \frac{1}{\sqrt{n!}} \begin{vmatrix} \phi_1(x_1) & \phi_2(x_1) & \cdots & \phi_n(x_1) \\ \phi_1(x_2) & \phi_2(x_2) & \cdots & \phi_n(x_1) \\ \vdots & \vdots & & \vdots \\ \phi_1(x_n) & \phi_2(x_n) & \cdots & \phi_n(x_n) \end{vmatrix} \tag{18}$$

The factor $1/\sqrt{n!}$ is a normalization factor. A Slater determinant $\psi(x_1, x_2, ...x_n)$ can be written in short form which includes the normalization constant and only shows the diagonal elements of the determinant,

$$\psi(x_1, x_2, ...x_n) \equiv \left|\phi_1(x_1)\phi_2(x_2)...\phi_n(x_n)\right\rangle \tag{19}$$

The antisymmetric property of a Slater determinant is $\left|...\phi_i...\phi_j...\right\rangle = -\left|...\phi_j...\phi_i...\right\rangle$.

Notation for One- and Two- Electron Integrals: If $\hat{P}$ is any quantum mechanical opterator for the property *P*, the expectation value of property *P*, denoted $\langle P \rangle$, for the system described by the wavefunction ψ is defined by

$$\langle P \rangle = \int \psi^* \hat{P} \psi d\tau \equiv \langle \psi | \hat{P} | \psi \rangle \tag{20}$$

When the wavefunction ψ is expressed in a Slater determinant form (Eq. 11) the matrix element P_{ij} is defined as

$$P_{ij} = \int \phi_i \hat{P} \phi_j d\tau \equiv \langle \phi_i | \hat{P} | \phi_j \rangle \tag{21}$$

The notation for two-electron integrals over orbitals is

$$\int dx_1 dx_2 \phi_i^*(x_1)\phi_j^*(x_2)\frac{1}{r_{12}}\phi_k(x_1)\phi_l(x_2) = \left\langle \phi_i\phi_j \middle| \phi_k\phi_l \right\rangle = \left\langle ij \middle| kl \right\rangle \tag{22}$$

2.2.3 The Hartree-Fock Equations

The Hartree-Fock theory considers the single determinant formed from electrons' orbitals as the best possible approximation to the ground state of the N-electron system described by an electronic Hamiltonian $\hat{H}$. The variational principle states that if a normalized wavefunction $\left|\tilde{\phi}\right\rangle$ that satisfies the appropriate boundary conditions is given, the expectation value of the Hamiltonian is an upper bound to the exact ground state energy. That is, if $\left\langle \tilde{\phi} \middle| \tilde{\phi} \right\rangle = 1$ then

$$\left\langle \tilde{\phi} \middle| \hat{H} \middle| \tilde{\phi} \right\rangle \geq E_0 \tag{23}$$

The equality holds only when $\left|\tilde{\phi}\right\rangle$ is identical to the exact wavefunction $|\phi\rangle$. The problem of minimizing a function subject to a constraint of normalization is solved by Lagrange's method of undetermined multipliers. According to the variational principle, the best orbitals are those which minimize the electronic energy *E*, which is defined by

$$\begin{aligned} E &= \left\langle \psi \middle| \hat{H} \middle| \psi \right\rangle \\ &= \sum_a^N \left\langle a \middle| \hat{h} \middle| a \right\rangle + \frac{1}{2}\sum_{a,b}^N \left(\left\langle ab \middle| ab \right\rangle - \left\langle ab \middle| ba \right\rangle \right) \\ &= \sum_a^N h_{aa} + \tfrac{1}{2}\sum_{a,b}^N \left(J_{ab} - K_{ab} \right) \end{aligned} \tag{24}$$

Where $\hat{h}$ is a core-Hamiltonian for an electron, describing its kinetic energy and potential energy in the field of the nuclei and J_{ab} and K_{ab} is the coulombic energy and exchange energy, respectively. By a linear variational method, the orbitals can be

systematically varied with the constraint that they remain orthonormal until the energy E_0 is a minimum.

For a given single determinant $|\psi\rangle \equiv |\phi_1\phi_2 \ldots \phi_a\phi_b \ldots \phi_n\rangle$ the energy is a function of the orbitals f. We need to minimize E with respect to the orbital, subject to the contrants that the orbitals remain orthonormal;

$$\int dx(1)\phi_a^*(1)\phi_b(1) = \langle \phi_a | \phi_b \rangle = \delta_{ab} \tag{25}$$

Using the variational principle, the best orbitals that minimize E are obtained from

$$[\hat{h}(1) + \sum_{b=1}^{N} \hat{J}_b(1) - \hat{K}_b(1)]\phi_a(1) = \sum_{b=1}^{N} \epsilon_{ba}\phi_b(1) \tag{26}$$

The Coulomb operator, corresponding to the classical electrostatic interaction, is defined by

$$\hat{J}_b(1)\phi_a(1) = \left[\int dx_2 \phi_b^*(2) r_{12}^{-1} \phi_b(2)\right]\phi_a(1) \tag{27}$$

and the non-local potential operator describing the exchange term is defined by

$$\hat{K}_b(1)\phi_a(1) = \left[\int dx_2 \phi_b^*(2) r_{12}^{-1} \phi_a(2)\right]\phi_b(1) \tag{28}$$

Eq. (28) can be written in a short from of

$$\hat{F}|\phi_a\rangle = \sum_{b=1}^{N} \epsilon_{ba}|\phi_b\rangle \tag{29}$$

The Fock operator, $\hat{F}$, is an effective one-electron operator, describing the kinetic energy of an electron, the attraction of all the nuclei and the repulsion of all the outer electrons (via $\hat{J}$ and $\hat{K}$ operators) called the Fock operator, of the form

$$\hat{F}(1) = \hat{h}(1) + \sum_{b=1}^{N} \hat{J}_b(1) - \hat{K}_b(1) \tag{30}$$

Eq. (29) is not in the canonical eigenvalue form. The reason is that any single determinant wavefunction formed from a set of orbitals retains a certain degree of flexibility in the orbitals. It is always possible to find a unitary matrix U such that the transformation diagonalizes. A new set of orbitals $\{\phi_a^{'}\}$ can be obtained from an old set $\{\phi_a\}$ by a unitary transformation, *i.e.*, $\phi_a^{'} = \sum_b \phi_b U_{ba}$. Then Eq. (30) can be written in the canonical eigenvalue form without changing the expectation value of energy.

$$\hat{F} \left| \phi_a^{'} \right\rangle = \epsilon_a \left| \phi_a^{'} \right\rangle \tag{31}$$

where ϵ_a is the orbital energy of $\phi_a^{'}$. From Eq. (24) the total electronic energy *E* is given by

$$E = \sum_{a}^{N} \tfrac{1}{2}\left(h_{aa} + \epsilon_a\right) \tag{32}$$

Since the Fock operator has a functional dependence, through the Coulomb and exchange operators, on the solution of $\{\phi_i\}$ of the pseudo-eigenvalue equation, thus the Hartree-Fock equations are really nonlinear equations and will need to be solved by iterative procedures.

2.2.4 The Roothan Equations

Numerical solutions of Eq. (31) are usually found by expanding the orbitals in a basis set;

$$\phi_i = \sum_{\nu}^{M} c_{\nu i} \chi_\nu \tag{33}$$

In Eq. (33), the unknown HF orbitals ϕ_i are written as a linear expansion in M known basis function χ_ν. If the set of χ_ν's is complete, it would be an exact expansion. Eq. (31) can be thus written as

$$\hat{F}\sum_{\nu}^{M} c_{\nu i}\chi_\nu = \epsilon_i \sum_{\nu}^{M} c_{\nu i}\chi_\nu \tag{34}$$

Multiplying from the left by a specific basis function and integrating yields the Roothan-Hall equations which can be shown in a matrix form of

$$\sum_{\nu} c_{\nu i}\int dr_1 \chi_\mu^*(1)\hat{F}(1)\chi_\nu(1) = \epsilon_i \sum_{\nu} c_{\nu i}\int dr_1 \chi_\mu^*(1)\chi_\nu(1) \tag{35}$$

Two matrices are defined here as the overlap matrix **S** and the Fock matrix **F**. The Fock matrix **F** has elements

$$F_{\mu\nu} = \int dr_1 \chi_\mu^*(1)\hat{F}\chi_\nu(1) = \left\langle \chi_\mu \middle| \hat{F} \middle| \chi_\nu \right\rangle \tag{36}$$

and the overlap matrix **S** has elements

$$S_{\mu\nu} = \int dr_1 \chi_\mu^* \chi_\nu = \left\langle \chi_\mu \middle| \chi_\nu \right\rangle \tag{37}$$

Although the basis function $\{\chi_\nu\}$ are assumed to be normalized and linearly independent, they are not in general orthogonal to each other. The diagonal elements $S_{\mu\nu}$ are unity and the off-diagonal elements are numbers less than one in magnitude. Eq. (35) can thus be written in a short form of the Roothaan equations as

$$\sum_{\nu} F_{\mu\nu}c_{\nu i} = \epsilon_i \sum_{\nu} S_{\mu\nu}c_{\nu i} \quad i = 1,2,3...M \tag{38}$$

If a system is closed-shell, the sum over N occupied spin orbitals included an equal sum over those with the α spin function and those with the β spin function, *i.e.*, $\sum_{b}^{N} \rightarrow \sum_{b(\alpha)}^{N/2} + \sum_{b(\beta)}^{N/2}$, the Fock operator then has a form of

$$\hat{F}(1) = \hat{h}(1) + \sum_{a=1}^{N/2} 2\hat{J}_a(1) - \hat{K}_a(1) \tag{39}$$

The Fock matrix F is the matrix representation of the Fock operator in the basis $\{\chi_\mu\}$, i.e.,

$$\begin{aligned} F_{\mu\nu} &= \int dr_1 \chi_\mu^*(1)\hat{h}(1)\chi_\nu(1) + \sum_a^{N/2} \int dr_1 \chi_\mu^*(1)[2\hat{J}_a(1) - \hat{K}_a(1)]\chi_\nu(1) \\ &= H_{\mu\nu}^{core} + \sum_a^{N/2} 2\langle \mu a | \nu a \rangle - \langle \mu a | a \nu \rangle \end{aligned} \tag{40}$$

where a core-Hamiltonian matrix is integrals involving the one-electron operator describing the kinetic energy and the nuclear attraction of an electron. By inserting the linear expansion for the molecular orbitals into the two-electron terms one gets

$$\begin{aligned} F_{\mu\nu} &= H_{\mu\nu}^{core} + \sum_a^{N/2} \sum_{\lambda\sigma} c_{\lambda a} c_{\sigma a}^* \left[2\langle \mu\sigma | \nu\lambda \rangle - \langle \mu\sigma | \lambda\nu \rangle \right] \\ &= H_{\mu\nu}^{core} + \sum_{\lambda\sigma} P_{\lambda\sigma} \left[\langle \mu\sigma | \nu\lambda \rangle - \tfrac{1}{2} \langle \mu\sigma | \lambda\nu \rangle \right] \\ &= H_{\mu\nu}^{core} + G_{\mu\nu} \end{aligned} \tag{41}$$

P is the density matrix, $P_{\mu\nu} = 2\sum_a^{N/2} c_{\mu a} c_{\nu a}^*$, and **G** is the two-electron part of the Fock matrix. The Roothaan equations are nonlinear and can be written in a matrix form of

$$\mathbf{FC} = \mathbf{SC}\boldsymbol{\epsilon} \tag{42}$$

where **C** is an M×M square matrix of the expansion coefficient c_{vi} and **S** is a diagonal matrix of the orbital energies ε_i. The problem of non-orthogonal basis set could be solved by orthogonalizing the functions $\{\chi_\nu\}$ to obtain the transformed basis function $\{\chi_\nu'\}$. The transformed Roothaan equations is then obtained as

$$\mathbf{F'C'} = \mathbf{C'}\boldsymbol{\epsilon} \tag{43}$$

which can be solved for eigenvectors **C**' and eigenvalues ϵ by diagonalize **F**'. The procedure used to solve for the MO coefficients c_α, called the Self-Consistent-Field (SCF) method is presented in Figure 9. By making an initial guess at the spin orbitals, one can calculate the average field seen by each electron and then solve the eigenvalue equation for a new set of spin orbitals. Using these new spin orbitals, one can obtain new fields and repeat the procedure until self-consistency is reached.

The SCF procedure is as follow:

1. Specify a molecule and a basis set { χ_ν }.
2. Calculate all required integrals ($S_{\mu\nu}$, $H_{\mu\nu}^{core}$ and $\langle \mu\lambda | \nu\sigma \rangle$).
3. Diagonalize the overlap matrix **S**.
4. Obtain a guess at the density matrix **P**.
5. Calculate the Fock matrix from matrices **G** and **P**, and two electron integrals $\langle \mu\lambda | \nu\sigma \rangle$.
6. Diagonalize the Fock matrix to obtain **C** and ϵ.
7. Form a new density matrix **P** from **C**.
8. Determine whether the procedure has converged. If it has not converged, return to step (5) with a new **P**.
9. If the procedure has converged, use the resultant solution to calculate expectation values.

By repeating the calculation for different nuclear coordinates the potential energy surface for nuclear motion can be explored. The equilibrium geometry of a molecule can be determined by finding a set of nuclei's positions which minimize the total energy.

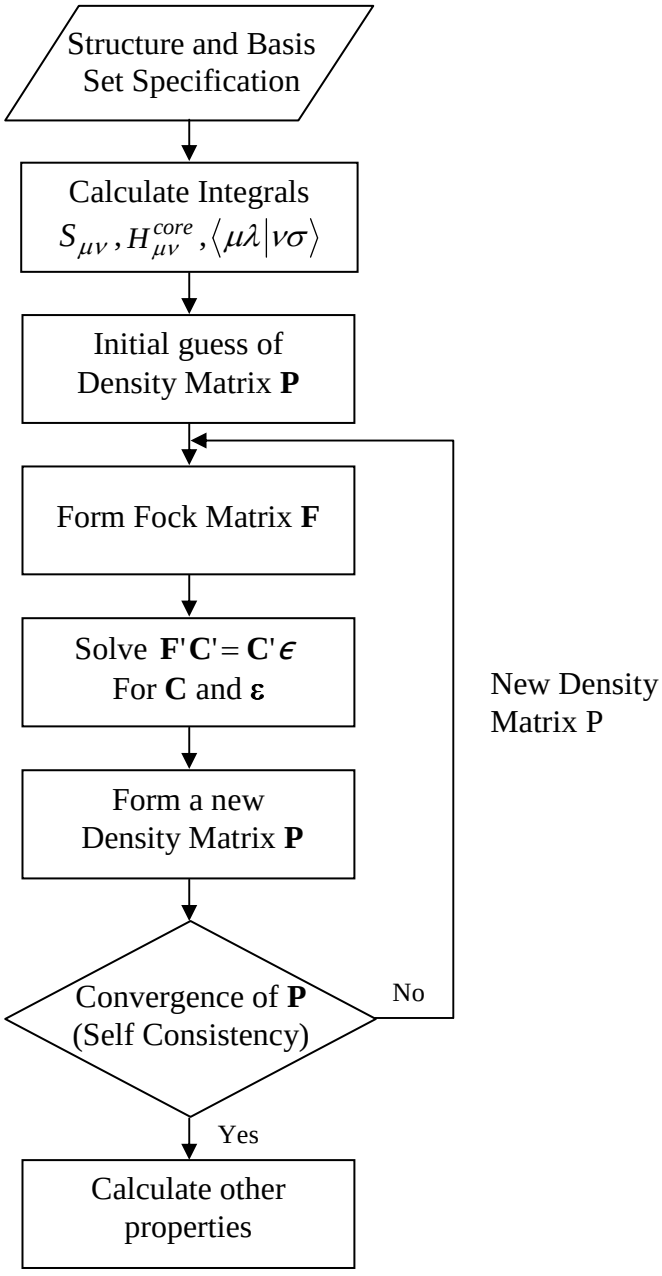

Figure 9 A self-consistent field procedure used to solve the wavefunctions of the Schrödinger equation.

2.3 Density Functional Theory (DFT)

Density functional calculations appear, at first glance, to be almost identical to ab initio Hartre-Fock calculations apart from having to choose a specific functional for the exchange and correlation to replace the Hartree-Fock functional. One solves a set of SCF equations in the same way as one does in ab initio Hartree-Fock calculations.

2.3.1 The Kohn-Sham Equations

The development of DFT in the area of computational chemistry dates from the mid 1960s when Hohenberg and Kohn demonstrated that the ground-state energy of a system of interacting electrons subject to an external potential $V(r)$ is a unique functional of the electron density Kohn *et al.*, 1965, and it can be obtained by minimizing the energy functional with respect to the density, $E = E[\rho(r)]$

$$E^{DFT} = \min_{\rho(r)} E[\rho(r)] \tag{44}$$

Later, Kohn and Sham demonstrated that there is an equivalence between the electronic density of this system (our real system) and that of a model system of noninteracting electrons which are subjected to an effective potential, V_{eff}. This provided a way to solve the problem of finding the density of the many-electron interacting system, via obtaining the electron density of the noninteracting system. This density can be expressed in terms of single electron orbitals, $\psi_i(r)$, known as Kohn–Sham (KS) orbitals,

$$\rho(r) = 2\sum_{i}^{occ.} \left|\psi_i(r)\right|^2 \tag{45}$$

where the sum extends over the occupied single-particle orbitals (here, we restrict to the most simple situation in which all orbitals are doubly occupied). Because of the relationship in Eq. 2, the energy functional can be expressed either in terms of the

density (Eq. 44) or the single-electron orbitals and the nuclear positions R_N of atoms in the system,

$$E^{DFT} = \min_{\{\psi_i\}} E^{KS}\left[\{\psi_i(r)\},\{R_N\}\right] \tag{46}$$

The energy functional can be written as:

$$E^{KS} = 2\sum_{i}^{occ.}\int \psi_i^*(r)\left(-\frac{\nabla^2}{2}\right)\psi_i(r)dr + \int V(r)\rho(r)dr$$
$$+\frac{1}{2}\int\frac{\rho(r)\rho(r')}{|r-r'|}drdr' + E_{xc}\left[\rho(r)\right] \tag{47}$$

The first term on the right-hand side of this expression is the kinetic energy of the noninteracting electrons. The second term corresponds to the interaction of the electrons with the nuclear charges and $V(r)$ is the potential as a result of the nuclei. Where only valence electrons are explicitly considered in the calculation, $V(r)$ is a pseudopotential. The third term corresponds to the classical Coulomb interaction of a density distribution ρ. The fourth term, $E_{xc}\left[\rho(r)\right]$, is a functional of the density that accounts for the remaining contributions to the electron–electron interaction.

The single electron orbitals $\psi_i(r)$ of Eq. 45 and Eq. 46 can be obtained by solving the following single-particle equations known as Kohn–Sham equations Kohn *et al.,* 1996,

$$\left(-\frac{\nabla^2}{2} + V(r) + \int dr'\frac{\rho(r)}{|r-r'|} + V_{xc}(r)\right)\psi_i(r) = \varepsilon_i\psi_i(r) \tag{48}$$

where ε_i are the eigenvalues of the matrix of Lagrange multipliers and are called the Kohn–Sham eigenvalues or Kohn–Sham orbital energies. $V_{xc}(r)$ is the exchange-correlation potential,

$$V_{xc}(r) = \frac{\delta E_{xc}\left[\delta\rho(r)\right]}{\delta\rho(r)} \tag{49}$$

2.3.2 Local Density Approximation (LDA)

All terms in Eq. 47 can be calculated exactly, except $E_{xc}[\rho(r)]$ for which the DFT does not provide an explicit form. The theory only demonstrates that a universal expression for it exists, $E_{xc}[\rho(r)] = \int \rho(r)\varepsilon_{xc}[\rho(r)]dr$. Usually, $E_{xc}[\rho(r)]$ is taken as the exchange and correlation energy of a uniform electron gas, which is precisely known. This is the basis of the so-called local density approximation (LDA). In this approximation, it is assumed that the exchange and correlation energy of an electron at a point depends on the density at that point instead of the density at all points in the space Ziegler 1991. One of the main drawbacks of LDA is that van der Waals interactions, which originate from correlated motions of electrons caused by coulomb interactions between distant atoms, cannot be properly described. Therefore, special care should be taken when addressing problems in which van der Waals interactions might play a relevant role, such as stacking interactions between π-systems and the diffusion of ligands in purely hydrophobic cavities.

An extension of the LDA to unrestricted cases or open-shell systems (i.e., electronic configurations in which electrons are not paired) leads to the local spin-density approximation (LSD). In this case, not only the total density ρ, but also the electron densities of the electrons with spin α and β (ρ_α and ρ_β, respectively) are employed in the formulation. For instance, the exchange-correlation energy is expressed as

$$E_{xc}^{LSD}\left[\rho_\alpha(r),\rho_\beta(r)\right] = \int \rho(r)\varepsilon_{xc}\left[\rho_\alpha(r),\rho_\beta(r)\right]dr \qquad (50)$$

A useful property to describe where α and β electrons are localized in a given system (a molecule, a molecule–ligand complex, solid, etc.) is the distribution of the spin density, i.e., the difference $\rho_\alpha(r) - \rho_\beta(r)$. For a system in which all electrons are paired (e.g., a closed-shell system) the spin density is zero at all points in space. However, any system with unpaired electrons will show regions of nonvanishing spin density. The integral of the spin density over all space (i.e.,

$\int_r \left[\rho_\alpha(r) - \rho_\beta(r)\right] dr$) gives the total number of unpaired electrons (i.e., zero for a singlet state, one for a doublet state, two for a triplet state, etc.).

2.3.3 Generalized Gradient Approximation (GGA)

The accuracy provided by the local (spin) density approximation is not enough for most applications in chemistry and biology. One of its main drawbacks is that bond distances and binding energies can have large errors that appear in a nonsystematic way. This represents a serious problem for the study of ligand–protein interactions.

A step forward with respect to LDA is the so-called generalized gradient approximation GGA. This approach is based on using not only the density, but also the gradient of the density in the functional expression Becke 1986 in order to account for the nonhomogeneity of the true electron density. The functional can be generically written as,

$$E_{xc}^{GGA}\left[\rho_\alpha, \rho_\beta\right] = \int f(\rho_\alpha, \rho_\beta, \nabla\rho_\alpha, \nabla\rho_\beta) dr \tag{51}$$

Several forms for the explicit dependence of the integrand f on the densities and their gradients have been proposed, including semiempirical functionals that contain parameters that have been calibrated against reference values, usually using experimental data. In practice, E_{xc}^{GGA} is usually split into two terms corresponding to its exchange and correlation contributions (i.e., $E_{xc}^{GGA} = E_x^{GGA} + E_c^{GGA}$) and separate forms for each term are provided. Among the most popular GGA exchange and correlation functionals used in chemical applications are the ones denoted as BP86 (exchange part by Becke Becke 1986 and correlation by Perdew Perdew 1986, BLYP (combination of Becke exchange and correlation developed by Li, Yang and Parr Lee *et al.*, 1988), PBE (developed by Perdew, Burke and Ernzerhof in 1996 Perdew 1986).

The use of the GGA approximation improves considerably the description of bonding (and especially hydrogen bonding) with respect to pure LDA with a very low additional computational cost. The description of weak van der Waals interactions, however, remains problematic. Most of the applications of DFT to systems of interest use the GGA approximation. In summary, DFT provides a framework to find the total energy of a many electron interacting system by means of solving the one-electron equations of a model noninteracting system that shares the same density. Based on the generalized gradient corrections approximation and choosing a suitable exchange correlation potential, many problems of chemistry, physics, and biology can be addressed.

2.3.4 Hybrid Functionals

Hybrid functionals, which includes to some extent exact exchange energy in the functional expression, are also widely used. From the Hamiltonian equation and the definition of the exchange-correlation energy, an exact connection can be made between the E_{xc} and the corresponding potential connecting the non-interacting reference and the actual system. One of the most popular is B3LYP (exact exchange developed by Becke Becke 1993, combined with the LYP correlation functional). The exchange-correlation energy has the form of

$$E_{xc}^{B3LYP} = AE_X^{Slater} + (1-A)E_X^{HF} + B\Delta E_X^{Beck} + (1-C)E_C^{VWN} + CE_C^{LYP} \quad (52)$$

where the exchange includes the Slater exchange E_X^{Slater}, or local spin density exchange, along with corrections involving the gradient of the density and the correlation is provided by the LYP Lee *et al.*, 1988 and VWN by Vosko, Wilk and Nusair Vosko *et al.*, 1980 correlations. The constants A=0.80, B=0.72, and C=0.81 are determined by Becke by fitting to the G1 molecule set Becke 1993.

ONIOM approach

The theoretical treatment of large molecular systems has made tremendous progress during the few years. Especially the development of reliable functionals in the framework of density functional theory (DFT) in combination with efficient schemes for the evaluation of coulomb and exchange integrals have led to theoretical methods that scale almost linearly with the size of the system. However, the accurate ab initio modeling of chemical systems containing a large number of atoms is still a challenging task. Especially the theoretical description of chemical reaction, i.e. the accurate modeling of transition states, requires methods that are usually not applicable to large molecules. There are several remedies to circumvent this problem. Often small model systems are used to describe the reaction center that is usually concentrated in a particular region of the molecule (Morokuma *et al.*, 1991). Another approach uses simplified Hamiltonians like in semiempirical and molecular mechanics methods. However, the parametrization process and can not be generalized.

An obvious solution to this problem is the partitioning of the system into two or more parts or layers, where the interesting or difficult part of the system (the inner layer) is treated at a ‘high’ level of theory and the rest of the system (the outer layer) is described by a computationally less demanding method. This idea is not new and many different implementations can be found in the literature. These hybrid methods differ mainly in two aspects. First, there are different ways to treat the boundary region of the different parts of the molecule. If there is no covalent bond between the layers, there is no special boundary region. A typical case is a solvated system, where the solvent molecules form the outer layer and the solute is the inner part which is treated by a higher level method. However, if one is interested in the accurate description of a particular region of a large organic molecule or a macromolecule, covalent bonds have to be cut in order to generate the inner model system. This process leaves dangling bonds at the border of the inner layer, which have to be saturated in order to avoid a chemically unrealistic model. Therefore, so-called link atoms--usually hydrogen atoms--are introduced. They are only present in the model

system and their treatment differs in the different implementations that have been published.

The second curial aspect in all the hybrid schemes is the interaction between the inner and outer part of the system. If the total energy $E(X,Y)$ of the entire system $X-Y$ (inner region X, outer region Y) is defined as

$$E(X-Y) = E_{High}(X) = E_{Low}(Y) + E_{Interlayer}(X,Y) \tag{53}$$

with $E_{Interlayer}(X,Y)$ being a separate interaction energy between the two layers, this may be referred to as a 'connection scheme'. On the other hand, if the total energy $E(X,Y)$ is calculated according to

$$E(X,Y) = E_{Low}(X-Y) - E_{Low}(X) + E_{High}(X) \tag{54}$$

then we shall refer to it as an 'embedding or extrapolation scheme'. In the latter case there is no necessity for a special interaction Hamiltonian, since the interaction between the two layers is consistently treated at the low level of theory. Obviously, both approaches are equivalent, if

$$E_{Low}(Y) + E_{Interlayer}(X,Y) = E_{Low}(X,Y) - E_{Low}(X) \tag{55}$$

i.e. if $E_{Interlayer}(X,Y)$ corresponds to the exact interaction energy at the respective low level. The ONIOM method (including IMOMM and IMOMO) method is an extrapolation scheme. A molecular system can be divided into up to three different layers do not have to be inclusive, i.e. the outermost layer can be connected directly to the innermost one. Every layer can be treated at an arbitrary level of theory. Geometry optimizations can be characterized by the integrated Hessian evaluation. The ONIOM method has been implemented into the Gaussian98 program system (Frisch *et al.*, 1998).

Details of calculations

1. Faujasite zeolite

For the faujasite zeolite, the active site is represented by the 84T cluster (Figure 12), including 297 atoms of the two interconnecting supercages forming a nanosized chemical reactor in which the adsorbates can be trapped inside, was taken from the lattice structure of faujasite zeolite (Olson *et al.,* 1969). The ONIOM3 scheme in which the whole model is subdivided into three layers is adapted for computational efficiency. The active region consisting of the 3T cluster, $H_3SiOAl(OH)_2O(H)SiH_3$, which is considered the smallest unit required to represent the acid site of zeolite and the reactive molecules, is treated with the MP2/6-31G(d,p) method. In the 3T cluster, one of the silicon atoms in the faujasite zeolite is substituted by an aluminum atom, and a proton is added to one of the bridging oxygen atoms bonded directly to the aluminum atom, conventionally called the O1 position (Hill *et al.,* 1999). The extended framework environment is included using less expensive levels of theories, the Hartree–Fock, and molecular mechanics force field (UFF) methods (Rappe *et al.,* 1992). The HF/3-21G method is used for the 9T ring fragment connecting the 3T acidic site to complete the 12T pore opening of the faujasite zeolite. The rest of the extended framework is treated with the UFF force field to reduce the required computational time and to practically represent the confinement effect of the zeolite pore structure.

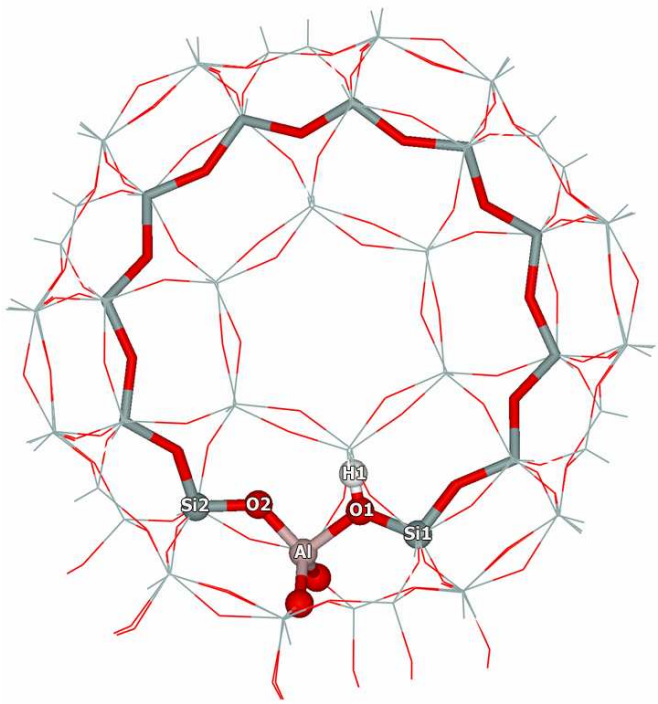

a)

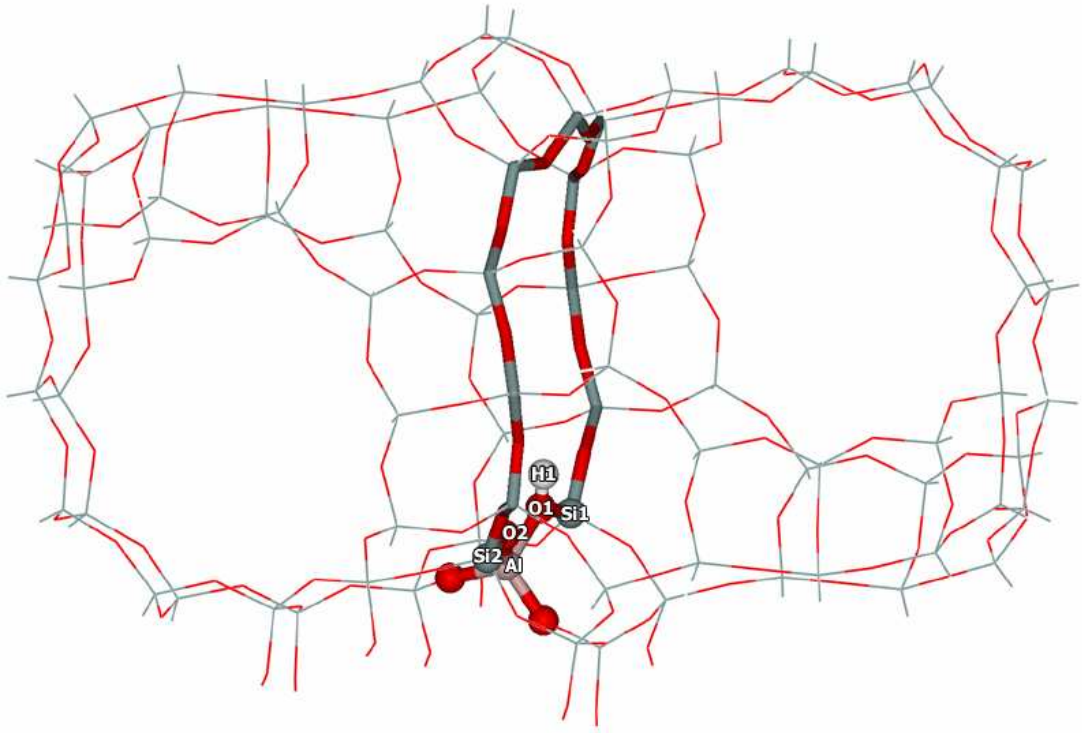

b)

Figure 10 ONIOM3 layer of 84T cluster models of faujasite. Atoms belongings to the 12T quantum cluster are drawn as bonds and sticks. (a) Front view, (b) side view.

The calculations have been performed by using the Gaussian98 code (Frisch *et al.*, 2001). The basis set for the Hartree–Fock calculations is 3-21G, while the 6-31G(d,p) basis set is used for the MP2 calculations. During the structure optimization, only the active site region [≡SiO(H)Al$(O)_2$OSi≡] and the adsorbates are allowed to relax. In order to obtain more reliable interaction energies, the single-point energy calculations at the ONIOM(MP2/6-311++G(d,p):HF/6-31G(d):UFF)//ONIOM (MP2/6-31G(d,p):HF/3-21G:UFF) level are carried out and basis set superposition error (BSSE) corrections are also taken into account.

2. ZSM-5 zeolite

The active site of H-ZSM-5 zeolite is represented by two different cluster sizes: 5T and 46T clusters, which are shown in Figure 13. The first model consists of five tetrahedral atoms [$(H_3SiO)_3$Al(OH) SiH_3] which are located at the cross section of the straight channel and zigzag channel and are consequently considered as the active region that allows the adsorbate molecules to react with the Brønsted proton. In this cluster, all atoms except the dangling hydrogen atoms, which are constrained in Si-O directions in the framework of the ZSM-5 zeolite, including the adsorbate molecules, are fully relaxed to replicate the real reaction phenomena. The second cluster was modeled by the two-layered ONIOM model. During the optimization, only the 5T regions [$(≡SiO)_3$Al(OH)Si≡] with the adsorbate molecules are allowed to relax since it has been pointed out that full relaxation of zeolite clusters can lead to structures that deviate largely from the experimental zeolite geometries (Brand *et al.*, 1993). This model has also been validated in our previous studies (Namuangruk *et al.*, 2004, 2005) and also in this study to give reasonable adsorption energies which compared well with the experimental measured values.

The ONIOM scheme has been implemented on the extended 46T cluster model to represent the zeolite pore cavity and zeolite framework, which includes the 10-membered ring channel containing the active region (represented as balls and sticks in Figure 13), as in the 5T cluster. The consequence of this is that the results obtained are anticipated to clarify the effect of the zeolite framework.

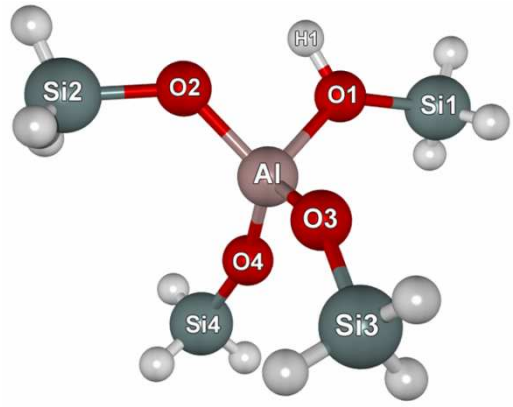

a)

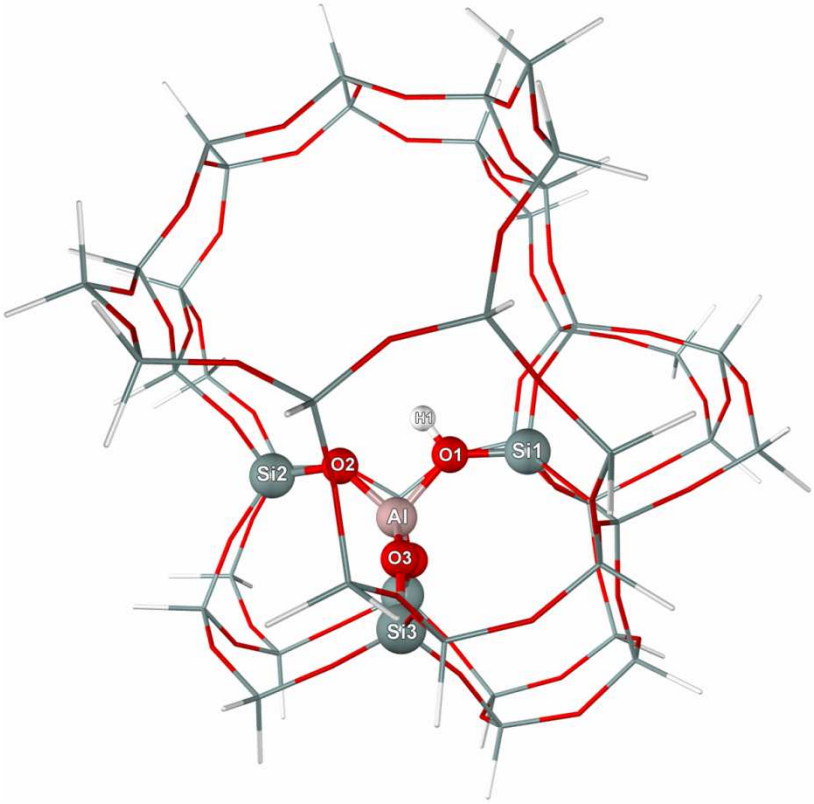

b)

Figure 11 The 5T and 46T clusters represent the active site of ZSM-5 zeolite in the zigzag channel view. The ball-and-stick graphics illustrates the relaxed geometry resulting from calculations at B3LYP/6-31G(d,p), the lines from the universal force field (UFF).

The calculations related ZSM-5 zeolite models were performed by the Gaussian03 program (Frisch *et al.*, 2001, 2004). The adsorbate molecules and 5T cluster of the first model, as well as the 5T region of the ONIOM model, were treated by the B3LYP (Becke 1993, Lee *et al.*, 1988, Stephens *et al.*, 1994) density functional theory at 6-31G(d,p), while the rest of the framework is treated with the universal force field, UFF (Rappe *et al.*, 1992).

3. Carbon Nanotube

The perfect and the Stone–Wales defective sites on the sidewall of (5,5) armchair single-wall carbon nanotube (SWNTs), where the latter site is formed by a rotation of the p-bond by 90 degrees with respect to the perfect one, are modeled to study the decomposition of nitrous oxide (see Figs. 14a and b). A finite length of the armchair (5,5)-SWNT containing 90 carbon atoms was carefully selected to be representative of the SWNTs. The dangling bonds at the end of the fragment tube are terminated by hydrogen atoms giving a $C_{90}H_{20}$ model. It can be seen that there are two types of nonequivalent C–C pair sites, the 1,2-pair site and the 2,3-pair site on the sidewall of carbon nanotubes. However, the 1,2-pair site was verified to have a higher reactivity than the 2,3-pair site (Long *et al.*, 2003, Lu *et al.*, 2003b, Lu *et al.*, 2002b) in chemical functionalizations of the SWNTs. Therefore, the data reported in this part of thesis were obtained from the $C_{90}H_{20}$ complete Clar network model at the 1,2-pair site. All calculations were carried out at the B3LYP level of theory with the 6-31G(d) basis set. Full optimizations and electronic population analysis of all stationary structures in the reaction pathways were carried out by the Gaussian03 code (Frisch *et al.*, 2001).

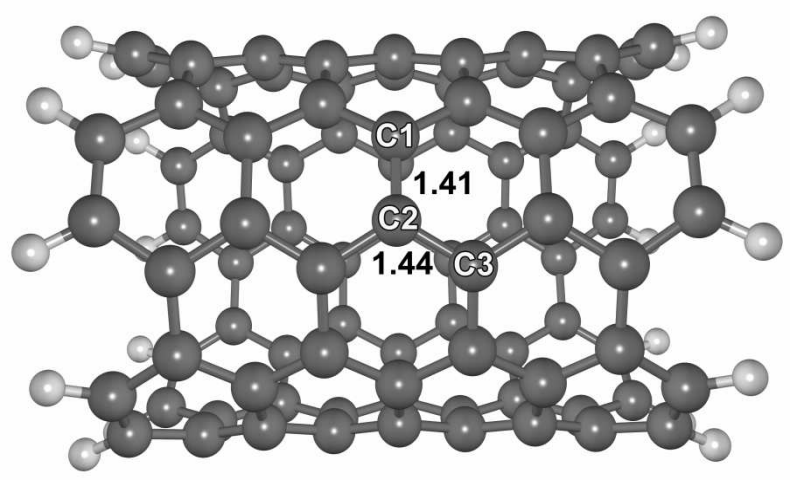

a)

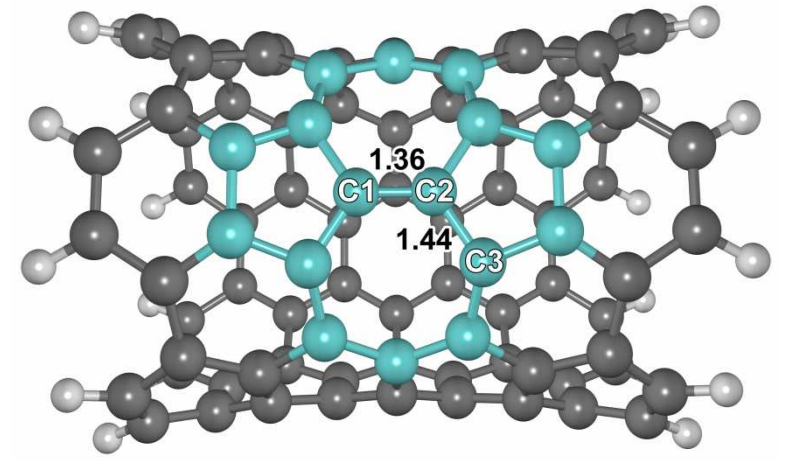

b)

Figure 12 Representation of the fragment tube of (a) perfect and (b) defective armchair (5,5)-SWNTs calculated at B3LYP/6-31G(d).